OPTICAL TACTILE ARRAY SENSOR FOR LUMP DETECTION IN SOFT TISSUE

by

Mustafa Zahid YILDIZ

B.S. in Electrical and Electronics Engineering
Sakarya University, 2004

Submitted to Institute of Biomedical Engineering
in partial fulfillment of the requirements
for the degree of
Master of Science
in
Biomedical Engineering

Boğaziçi University
September 2007

OPTICAL TACTILE ARRAY SENSOR FOR LUMP DETECTION IN SOFT TISSUE

APPROVED BY:

Assist. Prof. Dr. Burak GÜÇLÜ.....
(Thesis Advisor)

Assist. Prof. Dr. Ata AKIN.....

Assist. Prof. Dr. Çağatay BAŞDOĞAN.....

DATE OF APPROVAL: 21.10.2007

ACKNOWLEDGEMENT

I would like to thank my supervisor Assist. Prof. Dr. Burak Güçlü for his friendly guidance and his great contribution to my thesis. I am especially grateful to him for giving me especially moral support and also financial support, and being patient with me during my research.

I would like to thank Assist. Prof. Dr. Çağatay Başdoğan from Koç University Mechanical Engineering Department for letting me work in his Robotic Laboratory and giving me some valuable ideas for future work.

I would like to express my special thanks to my fellow colleagues, Biomedical Engineering Assistants for their friendship, and especially Didar Talat and A. Deniz Duru for their support.

This thesis is dedicated to my family who has supported me all through my life.

ABSTRACT

OPTICAL TACTILE ARRAY SENSOR FOR LUMP DETECTION IN SOFT TISSUE

Tactile information has great importance in many areas. Receiving tactile information from a slave-robot is a necessary component of tele-detection with tactile display. Surgeons highly depend on tactile feedback in minimally invasive surgery to locate arteries and tumors hidden in tissue. Additionally physicians use palpation for a variety of medical procedures to find tumors and arteries, as well as to assess the health of soft tissue. For these applications, tactile sensors can provide objective, quantitative, and consistent measurements. The tactile feedback may restore the lost tactile sensation as well.

Determining a palpable suspicious abnormality needs continued monitoring and requires maintaining a record of the examination results, but at present verbal notes are used and they are limited to subjective information about the position, size, and hardness of the lump. Because it is difficult to verbalize tactile sensations, tactile sensors should be used for quantitative measurements.

In this study, an optical tactile array sensor has been developed. It has advantages over pre-existing discrete tactile sensors in terms of pattern recognition and sensing a pressure distribution over an area. The deformation of elastic silicon-rubber surface was measured optically. It can be used in breast tumor identification which has been conventionally done by hand palpation. The tactile probe can detect lumps in soft tissues and can also draw a map of the sample. This map can be fused on a real picture of the tissue to determine the probable location.

The sensor consisted of 5x5 phototransistor array, 4x4 infra-red light sources, and silicon-rubber elastic surface. Each sensor output was selected by using a 16-bit multiplexer and the output signal was detected by a data-acquisition card. The software

was developed in MATLAB. The sensor produces an image which shows the contact surface and quantitative and visual results are presented to the user.

The sensor has a wide dynamic range (1 to 750 g), and high linearity (R^2=0.927). The tactile sensor was tested with two phantoms, 7 different Von Frey Hairs and fingertip contact experiments.

Keywords: Tactile array sensor, lump detection, tactile mapping, palpation, optical sensor.

ÖZET

YUMUŞAK DOKUDA YUMRU ALGILAMAK İÇİN OPTİK DOKUNSAL ALGILAYICI DİZİSİ

Dokunsal bilginin pek çok alanda büyük önemi bulunmaktadır. Köle-robottan dokunsal bilgi almak dokunsal görüntüleme ile uzaktan tespit için gerekli bir bileşendir. Cerrahlar minimal girişsel ameliyatlarda dokuda kaybolan damarları ve tümörleri bulmada dokunsal bilgiye çok fazla ihtiyaç duymaktadır. Ek olarak, doktorlar tümör ve damarları bulmada ve yumuşak doku değerlendirmesinde hastayı elle muayene etmektedir. Bu uygulamalarda, dokunsal algılayıcılar nesnel, nicel ve tutarlı bilgi sağlayabilirler. Ayrıca, dokunsal geribildirim kaybolmuş olan dokunsal duyuyu da yeniden kazandırabilir.

Elle hissedilebilen şüpheli bir anormallik sürekli takip ve muayene sonuçlarının kaydını gerektirir, fakat bildirilen sözel şikayetler, şişliğin yeri, büyüklüğü ve sertliği hakkında öznel bilgi vermektedir. Dokunsal hisleri ifade etmenin zorluğunda dolayı, nicel ölçümler için dokunsal algılayıcılara ihtiyaç vardır.

Bu çalışmada, optik dokunsal algılayıcı dizisi geliştirilmiştir. Bu algılayıcının örüntü tanıma ve basınç dağılımını algılama gibi ayrık dokunsal algılayıcılara sahip olma gibi avantajları vardır. Elastik silicon-kauçuk yüzeyin deformasyonu optik olarak ölçülmüştür. Bu algılayıcı konvansiyonel olaral elle yapılan meme kanseri tespitinde kullanılabilir. Dokunsal sonda yumuşak dokudaki yumruları saptayabilmekte ve bakılan alanın bir haritasını çıkarabilmektedir. Bu harita, dokunun gerçek bir resmi ile birleştirilerek olası yeri saptamada kullanılabilir.

Algılayıcı, 5x5'lik bir fototransistör dizisi, 4x4'lük bir kızılötesi ışık kaynağı ve elastik silikon-kauçuk yüzeyden oluşmaktadır. Her algılayıcı çıkışı, bir 16-bit çoğullayıcı ile seçilmiştir ve çıkış sinyali bir veri-toplama kartı ile kaydedilmiştir. Yazılım MATLAB'de geliştirilmiştir. Algılayıcı, kullanıcıya temas alanını, nicel ve görsel sonuçları göstermektedir.

Algılayıcının geniş bir dinamik aralığı (1-750 gram-kuvvet) ve yüksek bir doğrusalığı (R^2=0.927) vardır. Algılayıcı iki fantom, 7 boyda Von Frey Tüycükleri ve parmak ucu kontakt deneyleriyle test edilmiştir.

Anahtar Sözcükler: *Dokunsal algılayıcı dizisi, yumru tespiti, dokunsal haritalama, dokunarak muayene, optik algılayıcı.*

TABLE OF CONTENTS

LIST OF TABLES

LIST OF FIGURES

LIST OF SYMBOLS

ε	The permittivity of the dielectric
A	The area of the plates
d	The spacing between plates
Ω	Ohm
R	Resistance
P	Resistivity
L	Length

LIST OF ABBREVIATIONS

MTS	Matrix Tactile Sensor
MIS	Minimally Invasive Surgery
IR	Infrared
LED	Light Emitting Diode
VFH	Von Frey Hairs
OTAS	Optical Tactile Array Sensor

1. INTRODUCTION

1.1 Motivation and Objectives

A fundamental problem in most of palpation systems, minimally invasive surgery systems and haptic devices is the lack of tactile feedback. Surgeons use palpation for a variety of medical-procedures- to find tumors and arteries, as well as assess the health of soft tissues. Minimally invasive surgical procedures prevent surgeons from using palpation directly. Haptics in the form of feedback and tactile sensors may be useful for this problem. Tactile sensors can provide objective, quantitative and consistent measurements [1-3].

Different sensing methods have been explored for robotic tactile sensing; few are suitable for clinical usage. A tactile sensor for medical palpation in minimally invasive surgery would share many engineering goals with industrial sensors but would also need to meet several requirements that are different from the majority of industrial uses. These needs include: compactness, clinical suitability for human sensing and ease of use/ergonomics [1].

Palpation is a procedure that surgeons exploit regularly and "naturally" in traditional surgery in order to estimate tissue hardness and to locate blood vessels hidden beneath opaque tissues. This is very important because the accidental puncturing of blood vessels during MIS is a rather frequent life threatening complication [4].

Physical breast examination is an effective and completely non-invasive method for the detection of breast cancer [5-6-7]. With a lump as the most common symptom of breast cancer, studies show that the majority of breast cancers were found by palpation which complements mammography, since palpation can evaluate breast tissue near the chest wall and axilia that is not accessible to mammography [7]. In addition, studies have found that as many as 12-15% of cancers that were detected by physical examination were not apparent on mammograms [5-7].

Unfortunately, breast palpation has been hampered by problems inherent in its subjective nature, leading to difficulty in interpreting and documenting the examiner's impressions of the perceived lump in terms of tumor characteristics [7]. For example, a physician may determine that a palpable suspicious abnormality needs continued monitoring. This requires maintaining a record of the examination results, which at present is limited to verbal notes about parameters such as the position, size, and hardness of the lump. Because it is difficult to verbalize tactile sensations, the subjective and arbitrary nature of these notes makes effective follow-up exams problematic [5].

In this thesis, I aimed to understand problems with palpation and solve these practical problems by developing a novel tactile mapping device (TMD). This device should measure key variables during palpation: the examiner's search pattern, the applied forces, and the size and location of the lumps in the skin. It would be more convenient to integrate a three-dimensional camera that can track sensor motion and breast deformation in video speed, thereby fusing both tactile and camera images to locate lumps precisely in the soft tissue [1]. My objectives are (1) new tactile mapping technology can quantitatively measure the location and applied forces in palpation, and the tactile features of detected lumps; and (2) new device can accurately characterize and document lumps and can improve clinicians' ability to monitor changes in lumps across time. Most importantly, this Tactile Array Sensor can be used in haptic devices and tele-robotics systems, thereby making tele-palpation for breast cancer and tele-surgery with tactile-feedback possible.

From a set of "images" of the suspect mass, it is also possible to have a database and in the future a neural-network pattern recognition system may extract the certain properties of the lump, such as the depth and size, based on a nonlinear model of sensor-tissue interaction with hard inclusions. This TMD system can help to quantitatively and objectively record and characterize the findings of breast palpation. While the system is intended to perform breast examination in the clinical settings, eventually it may be used for self-examination by women through tele-home care [8-9].

1.2 Outline

In chapter 2, the physical principles of tactile sensors, types of tactile sensors, materials used in tactile sensor systems and previous works are explained comprehensively.

In chapter 3, all the methods that were used for both hardware and software design, statistical analysis methods, working principle of each part of the current sensor are presented in detail.

Chapter 4 includes the results of the experiments done by the current optical tactile array sensor and discussion about the results.

In Chapter 5, there is an overall conclusion which explains the benefits and drawbacks of the current optical tactile array sensor and future work.

2. BACKGROUND

2.1 The Need for Tactile Sensing

Tactile sensing is defined as continuous sensing of variable contact forces. At present, robots do not have tactile sensing ability, much in the same way that some humans lack tactile sensing because of disease or trauma. Thus both robotics and medicine should benefit from the development of improved tactile sensing [10].

2.1.1 Autonomous Robots

Robots are widely used to perform mundane repetitive tasks in many industrial and manufacturing settings. Most robots do not have any sensing capability; for those that do, the sensory abilities are primarily visual. Visual sensing technology is well developed. Although vision provides information on object location, it does not provide information on grip force. When a robot grasps an object, its hand can block its own vision. Enhancing tactile sensing in robots would improve their ability to manipulate objects without dropping or breaking them. It would improve performance in obscured environments such as murky water and smoke-filled rooms, where visual sensing would be limited. Providing robots with tactile sensing ability would make them more versatile, thus freeing human workers for more creative work [10].

Tactile and visual sensing complements each other well. Visual sensors can locate objects and measure their absolute position. Tactile sensors can sense local shape, orientation, and forces once the objects are grasped. Using visual sensing, it is only possible to discover mechanical properties by deducing them from optical properties. Using touch, we measure mechanical properties directly. Vision may guide the robot arm through many manufacturing operations, but it is the sense of touch that will allow the robot to perform delicate manipulations and assembly. Tactile sensing is needed when force, pressure, and compliance are important variables.

2.1.2 Teleoperation

The principle goal of telerobotics is to allow humans to extend to remote locations their ability to perform complex manipulative tasks. The prefix “tele” means “remote” or “at a distance”, and most telerobotics systems are called “teleoperators” or “remote manipulators”. These systems are especially useful in environments too hazardous for, or inaccessible to, humans. Examples include nuclear power plants, mines, space, rescue missions, handling electric transmission lines, and underwater work. Teleoperators recently recovered items from the 1912 shipwreck of the Titanic under 3.8 km sea [10].

The ability of humans to perform complex tasks depends on their sensory perception, motor control, and decision-making capabilities. A teleoperator couples human decision-making and motor control functions with the remote manipulator. The sensations that occur are directly fed back to the human operator, which improves dexterity, reliability, and ease. The enhanced capability allows the operator to cope with unforeseen situations.

Vision currently provides the most feedback to the operator. Some applications allow directly sight; in others, visual information is acquired remotely by television. For some applications, such as in murky water, neither direct vision nor television may be possible. For these we need a tele-touch system to mimic human tactile sensing capability at the remote site and to display the information to the human operator. The remote manipulator should be equipped with tactile sensors functionally similar to human tactile receptors. Telerobotic systems depend on, and benefit from, the decision making capabilities of human operator, so in the control sense they are easier to design than autonomous robotic systems. However, in telerobotic systems the tactile information must not only be obtained but also be displayed so that the operator can respond to the changes [10].

2.1.3 Medical Orthoses

We need tactile sensors to replace human touch and tactile sensors when natural tactile sensory abilities are impaired or lost. The sensory capabilities of the hands and feet may be reduced by injury or by many diseases, including diabetes, alcohol poisoning, and vascular disorders. Diabetes is the most common cause of neuropathy in the United States. Diabetes affects over one million people in the US, and about half of them suffer sensory loss in the hands and feet after living 25 years with the disease. Lack of sensations leads to abuse, tissue damage, ulcers, resorption of tissue, and sometimes amputation [10].

2.2 Discrete Versus Array Sensors

Individual or discrete sensors sense pressure at a point, but often we want to know the pressure distribution over an area. Array sensors can measure pressure distribution, and there are two ways to construct them. We can arrange N rows of M discrete sensors to form an NxM array. The second method is to lay strips of a conductive material at right angels to each other to form rows and columns. The cross points become the elements of the array. An array formed with strips requires fewer wires and therefore can be more compact than an array with the same number of elements formed with discrete sensors. However, an array formed with strips requires more complex conversion circuitry than an array formed with discrete sensors. Additionally, strip-formed arrays have greater cross-talk problems because the output of an individual array element may be contaminated by other elements on the same strip.

Discrete sensors operate singly and usually transmit a signal indicating a desirable change of environment (such as pressure) at the sensor. Discrete sensors can be formed into arrays that not only can detect these changes but can also produce an image of them.

2.3 General Tactile Sensor Requirements

The most commonly stated requirement is that a tactile sensor should be skin-like. This is a very qualitative requirement but again shows that human characteristics are often the models for designers of robots. Artificial skin should have high sensitivity, fast response, and continuously variable output, and it should require a little power and be cheap and durable. The desirable characteristics for robotic applications are similar to those for medical orthotic systems. A survey of researchers and industrial manufacturers by Leon D. Harmon of Case Western Reserve University led to the general requirements for tactile sensors listed below. For use on human hands and feet, sensors must also be flexible, soft, compact, comfortable, and nonintrusive.

- The spatial resolution should be 1-2 mm. This is approximately the spatial resolution of the human fingertip. Some applications, such as automated watch assembly, might require better than human fingertip resolution; for others, however, coarser resolution may be adequate.
- The force sensitivity should be 0.5-10g (5-100 mN). Of course the degree of sensitivity required depends on the application. Mass, velocity, acceleration, response time, and strength of materials are mutually dependent design parameters relevant to sensitivity requirements.
- A dynamic range of 1000:1 is desirable, and often a logarithmic response is satisfactory. That is, for small forces, high sensitivity is more important than it is for large forces.
- The sensor bandwidth should extent from dc to at least 100 Hz. Some robotics applications might require a bandwidth to 1 kHz. The bandwidth influences the overall frequency response of a control loop. The high-frequency requirements may be somewhat relaxed for sensors used on the fingertips, since the frequency components of human touch extend only up to about 20 Hz.
- Linearity is desirable, but some nonlinearity can be tolerated. As long as the sensor has good repeatability and stability, nonlinearity can be compensated.
- Hysteresis must be low. That is, the output should depend on only the input and not whether the input is increasing or decreasing.

- Sensors must be wear resistant, especially with slip. They must also be rugged to withstand industrial environments. Specialized applications could require extra durability with exposure to heat, radiation, electrical interference, smoke or mechanical abuse.
- Low-power consumption is important, especially for battery operated devices.

One of the most difficult aspects of sensor design is packaging. Lead breakage is a common problem. Lead wires must be attached to the sensors so that gripping forces do not break them. Both robotic and human hands have moving fingers, so lead wires must be flexible. To keep bulk reasonable, the number of lead wires must be minimal, and any electronics located near the sensors must be small [10].

Also overload protection is essential. Most commercial strain gages and pressure sensors do not have overload protection. Many of these are expensive, but even if they are not, the time necessary to replace and recalibrate them can be costly. Tactile sensor should be able to tolerate least double the largest pressure that we expect to encounter. The best tactile sensor designs should consider overload protection from the very start, perhaps in the form of mechanical stop.

2.4 Materials

Tactile sensing implies contact and contact transduction. Tactile sensors, by definition, sense mechanically in that the applied pressure deforms the contact material. We wish to transform this mechanical deformation into electrical signal that can be either simply displayed or digitized for further processing. The goal is a repeatable, linear relationships between pressure and electrical quantity such as voltage, current, resistance, inductance, capacitance or charge. These electrical quantities are determined by geometry, by dimensions such as length, thickness, and area, and by material properties such as resistivity, permittivity, and permeability. We can design pressure sensors that are based on varying any of these fundamental properties. The characteristics of all tactile sensors depend, to some degree, on the properties of the deformable contact material [10].

2.5 Analog versus Binary Sensation

The sensations perceived by robots depend on their functions. It is considered two forms of sensations. Binary sensation detects a pressure that exceeds a threshold and is usually used to initiate the grasping of a robot gripper. Analog sensation detects changes in pressure with time and is used for continuous processing of grip.

Binary sensing is easily carried out in a tactile system, but developing analog sensing is rather difficult process. The form of the output of an analog sensing device should be representative of the sensation. Most analog sensing devices produce an output that varies with time. Such output can be arranged in an image. The performance the driving system should remain stable when undesirable changes (such as temperature) occur.

2.6 Types of Tactile Sensors

2.6.1 Capacitive Tactile Sensors

Capacitive sensors are much more useful than inductive sensors as tactile pressure sensors. Applied pressure can easily vary the separation between the capacitor and plates and thus vary the capacitance [10].

Wang et al. [5] have presented a prototype tactile mapping device (TMD) system comprised mainly of a tactile sensor array probe (TSAP) which has capacitive elements. The probe is able to produce tactile maps of the breast pumps during a breast palpation. Focusing on the key tactile topology features from breast palpation such as spatial location, size and shape of the detected lesion, and force levels used to demonstrate the palpable abnormalities, these maps can record the results of clinical breast examination with a set of pressure distribution profiles and force sensor measurements due to detected lesion. These maps will serve as an objective documentation of palpable lesions for future comparative examinations.

They used a tactile sensor array probe (TSAP) which is composed of two crossed layers of copper strips separated by thin strips of silicone rubber [5,11]. Each crossing area forms a capacitor, and when a force is applied onto where the strips cross, the distance between the strips decreases and capacitance increases [5,12].

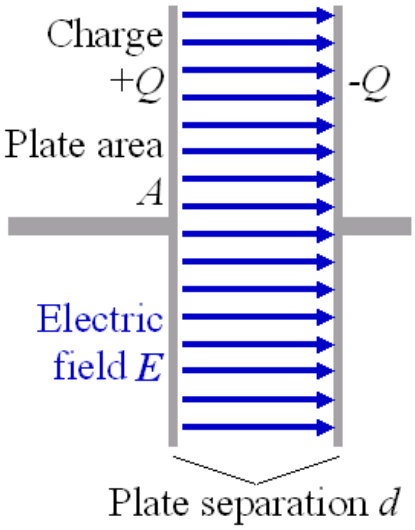

Figure 2.1 Capacitor symbol [5].

The capacitance of a parallel-plate capacitor is given by;

$$C = \frac{\varepsilon A}{d}; \qquad (2.1)$$

where ε is the permittivity of the dielectric, A is the area of the plates and d is the spacing between them (Fig. ‘2.1).

Specially designed electronics measure the capacitance of each element and relate the capacitance change to the force applied to each element. By measuring the capacitance variations from all the elements simultaneously, one can determine the spatial distribution of pressure across the sensor array. Figure 2.2 shows the operation of the capacitive tactile array sensor.

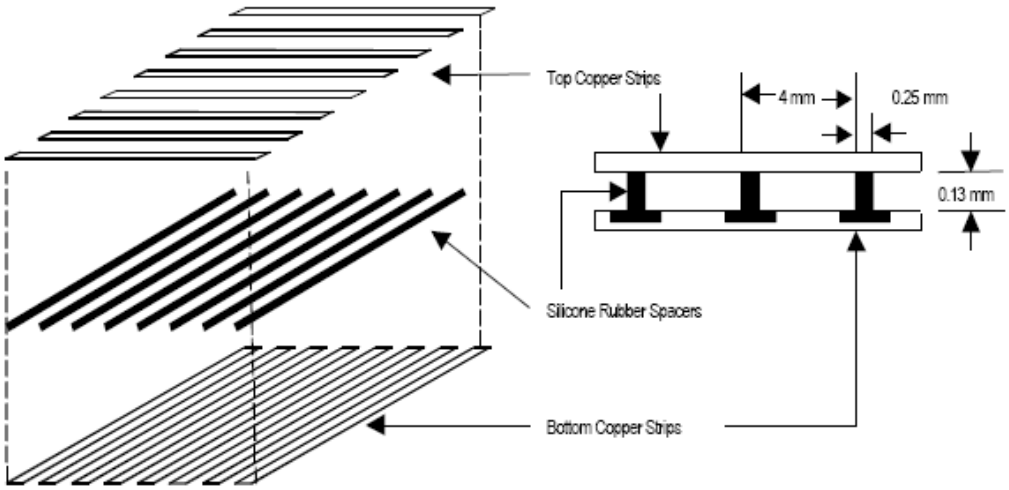

Figure 2.2 A drawing of a tactile array sensing [5].

The sensor array in Figure 2.2 is made with an inexpensive photolithography and etching process and can be easily attached to a variety of probe shapes. In this prototype specification, it is composed of an eight by eight tactile sensor with elements that are 4mm on a side. The sensor is mounted on a plastic brass backing plate with a surface that has been machined into a section of a square. The backing plate is 5.08 cm on a side and the effective sensing area is 3.20 cm on a side. The authors decided to make the sensor flat in order to minimize inhomogeneity because the resulting pressure distribution should have a uniform overall signal to noise ratio. The tactile images may then be consistent when used for various breast/chest background textures. The spatial resolution of the tactile array is 4 mm and where the smallest masses that they are interested to characterize are on the order of 1 cm in diameter. Smaller elements would increase spatial resolution at the cost of lower coverage area and low sensitivity since the capacitance is proportional to the element area [12]. Tactile sensor needs to be shielded from electromagnetic interference

The authors used also a Force/Torque Sensing System and a computer program written in C++ to measure six forces in Cartesian x-, y-, z- axes. Data was collected via the serial port of a computer.

From the breast model, data was collected. The models were made from Biolike^{TM} synthetic tissue that feels like a real breast [6]. They used two models in their tests. Each of them had 5 lumps that simulate easy- and hard-to-find breast tumors with various sizes and depths at different locations (Figure 2.3).

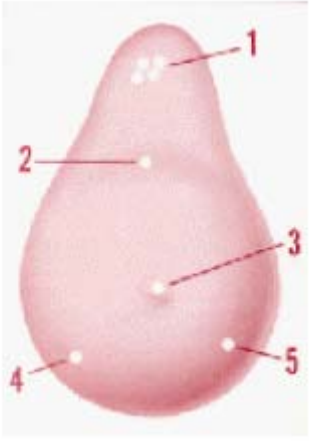

Figure 2.3 Breast models with simulated lumps [5].

Microsoft Visual C++ was employed to implement GUI to visually display pertinent data of TSAP (Tactile Sensor Array Probe) and force sensor.

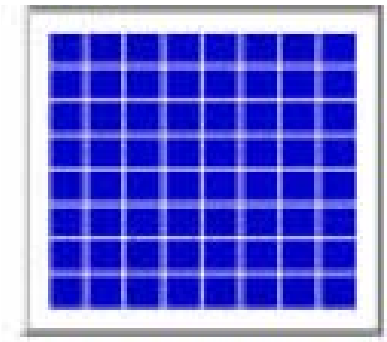

Figure 2.4 Pressure distribution provided by TSAP [5].

Each blue square on the Figure 2.4 corresponds to a tactile capacitive element. For tactile imaging of simulated lesions, the TSAP was used to acquire various tactile images by palpating the site after the examiner located the lesion by initial hand palpation. Since the relationship between the tactile images and lesion characteristics were expected to be complex and nonlinear, Wang et al. [5] stated that the inverse problem (extraction of lesion characteristics from tactile images) can be solved only when sufficient tactile information is provided.

Some of the outputs from the capacitive tactile array probe are shown in Figure 2.6. The peak points correspond to simulated lesions on the breast models shown in Figure 2.5.

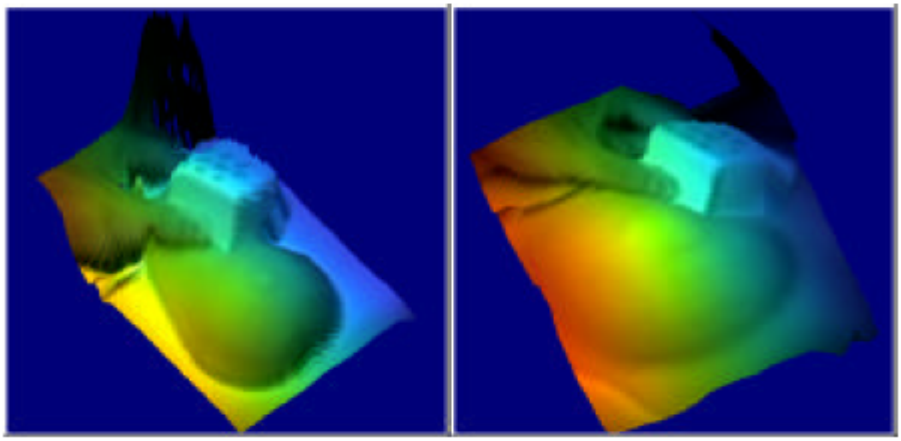

Figure 2.5 Breast model and tactile sensor to detect lesions [5].

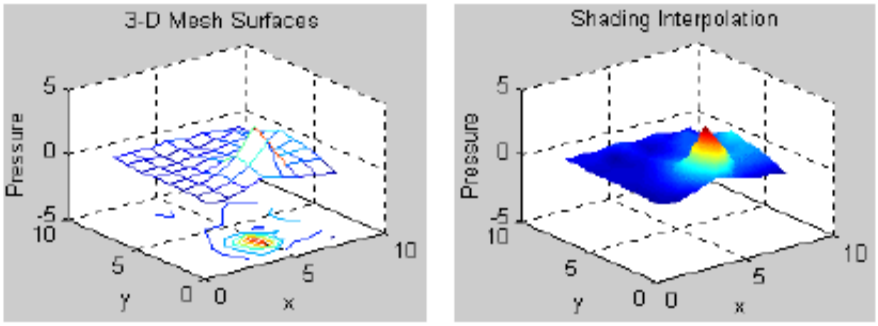

Figure 2.6 Capacitive tactile sensor output [5].

2.6.2 Tactile Sensors Using Strain-Gauge

A strain gauge is a device used to measure deformation (strain) of an object. The gauge is attached to the object by a suitable adhesive. As the object is deformed, the foil is deformed, causing its electrical resistance to change. This resistance change, usually measured using a Wheatstone bridge, is related to the strain by the quantity known as the *gauge factor*. Metal strain gauges are linear and accurate, but they are also expensive and difficult to apply.

The quantitative dependence of resistance on strain may be by noting the effect of strain on the parameters in the equation for resistance;

$$R = \frac{\rho L}{A} \tag{2.2}$$

Here R is the resistance, ρ is resistivity, L is the length, and A is the cross-sectional area.

Dargahi et al. [13] designed and tested a novel semiconductor microstraingauge endoscopic tactile sensor (Fig. 2.7). The designed assembly consisted of two semiconductor microstraingauge sensors, which were positioned at the back side of a endoscopic grasper. The sensor can measure, with reasonable accuracy, the magnitude and the position of an applied load on the grasper. The in-house electrical amplification system for the microstrain gauges was also designed, fabricated, and tested. The intensity of the magnitude of the applied force to the endoscopic grasper could be visually seen on a light emitting diode bar graph (Fig. 2.8).

Figure 2.7 Grasper used endoscopic surgeries [13].

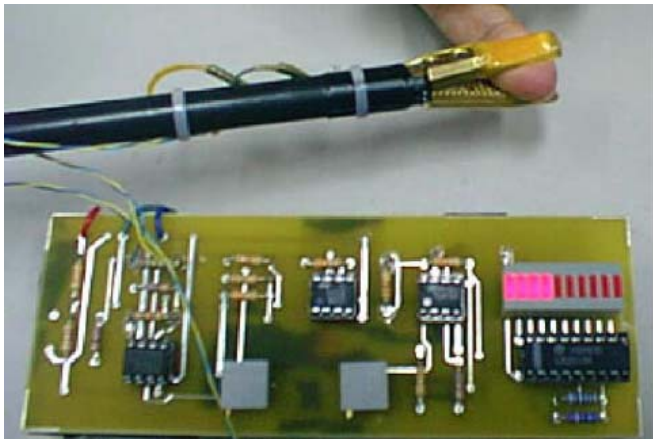

Figure 2.8 Microstraingauges mounted on the grasper and LED display for the applied force [13].

In total, 20 different force magnitudes, from 0.5 to 10 N with an increment of 0.5 N, at seven locations of the endoscopic grasper were tested experimentally (Fig. 2.9). The sensor had high force sensitivity, large dynamic range, and good linearity. It was insulated and could operate safely in wet environments. A 3-dimensional finite element modeling (FEM) was used to predict the behavior of the designed system under various loading conditions. There is a good correlation between the theoretical predictions of experimental results. Potentially, the miniaturized electronic device could be integrated with an endoscope and the complete system could be used in an operating room [13].

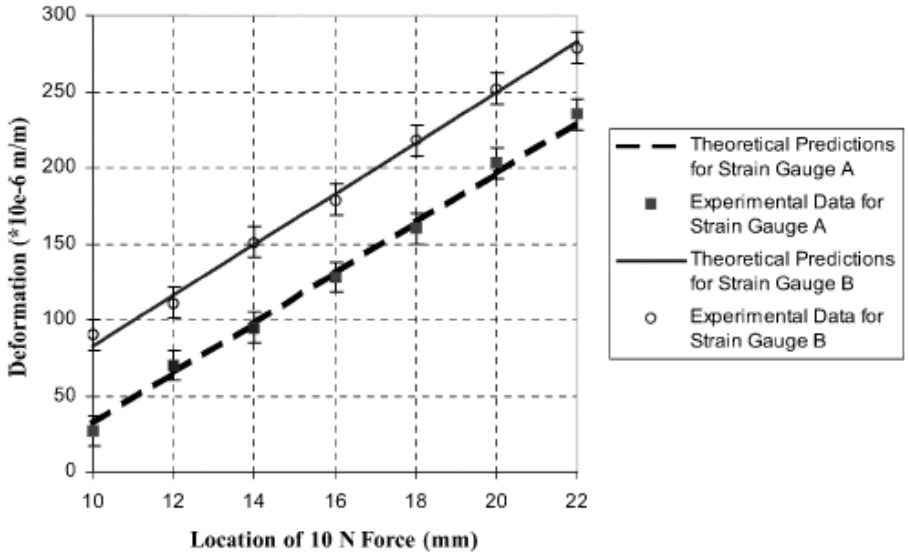

Figure 2.9 Force vs. deformation of an endoscopic strain gauge sensor [13].

With the rapid advances in biomedical technology and the refinement of numerous diagnostic and therapeutic techniques, non-invasive treatments and examinations have become quite common in clinic [19]. In fact, nowadays, minimally invasive surgery (MIS) has gained enormous popularity among the surgeons [14, 15, 16] and has opened up an exciting venue for research in the area of biomedical engineering. In MIS, surgical operation is performed with the help of a small endoscopic camera and several long, thin instruments through natural body openings or small artificial incisions [17, 18]. In comparison to the conventional open surgery, there exist several advantages for the patient:

less pain; less strain on the organism; reduction of trauma; faster recovery time; smaller injuries (aesthetic reasons); economic gain due to shorter recovery time; and reduction of post-operation complications [17]. The disadvantages of MIS include: restricted vision; difficult hand-eye coordination; lack of dexterity; and loss of tactile perception [20]. Among the disadvantages mentioned above, the loss of tactile perception has attracted a lot of attention [21–24]. It is well known that biological tissue composition and consistency are often changed from one tissue to another by various diseases [25]. In this regard, human palpation characteristics, such as force, compliance, and viscoelastic perceptions are of vital importance in all applications of MIS, especially in diagnostic and therapeutic endoscopic procedures [24, 26]. For instance, malignant tumors are generally harder than the surrounding tissue, and this is the reason why tumors can often be detected by palpation. Measuring the magnitude and location of the applied forces exerted by the endoscopic grasper is the fundamental requirement for the safe handling of biological tissues [27, 28].

In effect, to perform MIS more efficiently, a surgeon should be able to feel the tissues and detect the presence of blood vessels and ducts during the procedures. This ability is especially important during controlled manipulation tasks, for example, grasping of internal organs, gentle load transferring during lifting, removing tissues (e.g., gall bladder in laparoscopic surgery and loose bodies in knee arthroscopy), and suturing tissues together [29]. These capabilities coupled with the ability to detect various tactile properties demonstrate the importance of tactile sensing in MIS. Commercially available endoscopic graspers used in minimally invasive surgeries do not have any integrated tactile sensors; hence surgeons do not have any tactile feedback to manipulate the biological tissues safely. Thus, in order to enable the endoscopic surgeon to feel the tissues, sense the presence of blood vessels, and remove loose tissues from the operation site (such as, articulating joints) safely, tactile sensors should be incorporated into the endoscopic graspers [30].

Commercialized version of endoscopic grasper with a tactile sensor display is shown in the Figure 2.10.

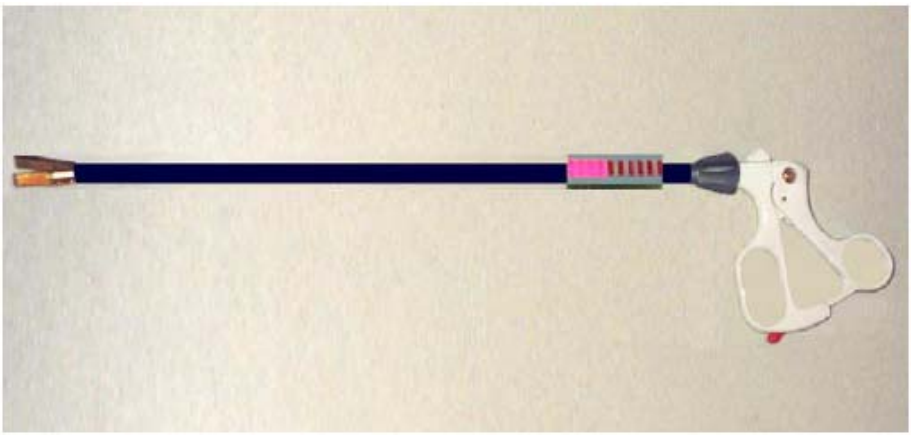

Figure 2.10 Commercial laparoscopy grasper with tactile sensor [13].

2.6.3 Optical Tactile Sensors

Optical tactile sensors usually detect a change in light intensity. Applied pressure can vary the distance that the light must travel from the source to the detector. In some optoelectronic pressure sensor designs, applied pressure moves or changes the shape of a part of the sensor which blocks some of the transmitted light. The intensity of the received light indicates the pressure. An optical sensor might be made smaller by using optical fibers to transmit the light from a remotely located source to a remotely located detector [10].

2.6.3.1 Phototransistors as sensitive elements:

A phototransistor is in essence nothing more than a bipolar transistor that is encased in a transparent case so that light can reach the *base-collector junction*. The phototransistor works like a photodiode, but with a much higher responsivity for light, because the electrons that are generated by photons in the base-collector junction are injected into the base, and this current is then amplified by the transistor operation. However, a phototransistor has a slower response time than a photodiode. There are some reasons to use phototransistors in some applications, these are;

- Low cost visible and near-IR photo detection,
- Available with gains from 100 to over 1500,
- Moderately fast response times,

• Available in a wide range of packages including epoxy coated, transfer molded, cast, hermetic packages, and in chip form,

• Usable with almost any visible or near infrared light source such as IR Leds; neon, fluorescent, incandescent bulbs; lasers; flame sources; sunlight; etc.

• Same general electrical characteristics as familiar signal transistors (except that incident light replaces base drive current).

As light source, there are several reasons to choose IR LEDs in most of applications;

IR LEDs are solid state light sources which emit light in the near-IR part of the spectrum. Because they emit at wavelengths which provide a close match to the peak spectral response of silicon photodetectors, both GaAs and GaAIAs IR LEDs are often used with phototransistors. Key characteristics and features of these light sources include:

• Long operating lifetimes,

• Low power consumption, compatible with solid state electronics,

• Narrow band of emitted wavelengths,

• Minimal generation of heat,

• Available in a wide range of packages including transfer molded, cast, and hermetic packages,

• Low cost.

Phototransistors can be used as ambient light detectors. When used with a controllable light source, typically an IR-LED, they are often employed as the detector element for opto-isolators and transmissive or reflective optical switches.

Ohka et al. [31] proposed an optical tactile sensor comprises an optical waveguide plate, made of transparent acrylic and was illuminated along its edge by a light source. The light directed into the plate remained within it due to the total internal reflection generated, since the plate was surrounded by air having a lower refractive index than the plate [32–35]. A rubber sheet featuring an array of conical feelers is placed on the plate to keep the array surface in contact with the plate. If an object contacted the back of the rubber sheet, resulting in contact pressure, the feelers collapsed, and at the points where these feelers collapsed, light was diffusely reflected out of the reverse surface of the plate because the

rubber had a higher refractive index than the plate. The distribution of contact pressure was calculated from the bright areas viewed from the reverse surface of the plate Figure 2.11.

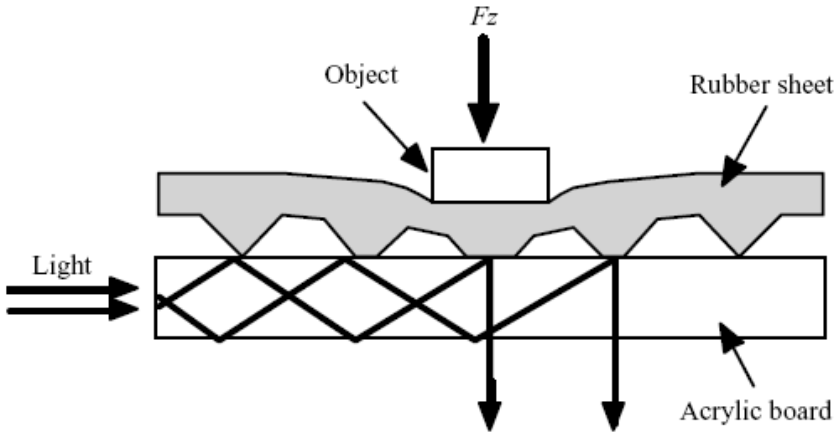

Figure 2.11 Diagram of an optical uni-axis tactile sensor [31].

The sensitivity of the optical tactile sensor could be adjusted by texture morphology and hardness of the sheet. The texture can be easily made fine with a mold suited for micromachining because the texture is controlled by adjusting the process of pouring the rubber into the mold. This process enables the production of a micro-tactile sensor with high density and sensitivity by using the abovementioned principle of the optical tactile sensor. However, this method could detect only distributed pressure applied vertically to the sensing surface and needs a new idea to sense the shearing force.

2.6.4 Vision Based Tactile Sensor

The vision-based tactile sensor capitalizes on available sophisticated vision system by translating haptic information into visual information [9, 13, 15].

Kamiyama et al. [37] developed a vision-based tactile sensor consisting of a transparent elastic body, blue and red markers inside the elastic body, and a color CCD camera. When a stress was applied on the surface, the internal strain of the body was optically measured by the movement of the markers. Finally force vector was calculated from the strain using elastic theory.

This proposed measuring method used information of strain of an elastic body. There are many choices about what kind of strain should be measured, and the approach adopted by Kamiyama et al. was to measure the horizontal movement of small markers in the elastic body, which were located at specified depths. To gather sufficient information for the reconstruction of the stress vectors, they used two layers of markers that are located at different depths (Fig 2.12). These layers could be distinguished by the colours of the markers (red and blue). They set the x-y plane parallel to the sensor surface and the z-axis extending vertically on the interior. By measuring these markers from a positive z direction with a CCD camera, they could obtain two sets of two dimensional motion vectors at different depths, so the amount of information was increased and the distribution of stress vector can be readily obtained [37].

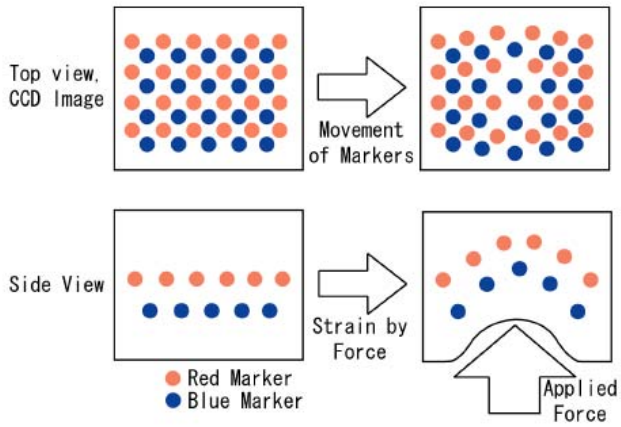

Figure 2.12 Vision-based tactile sensing system [37].

2.6.5 Piezoresistive Tactile Sensor

Matrix tactile sensor arrays (MTSA) have been often used in robotics to materials handing and manipulation with components. MTSA are specially fitted to be used in automated robotics assembly systems for evaluation forces to need to catch component, eliminating slide and protection from damage or destruction. The other field of application can be found very frequently in medical care, especially for orthopedical defects diagnostics.

Matrix tactile sensor arrays consist of mechanical part and electronics. For example, mechanical part consisted of 256 sensing elements, located in matrix of 16 rows and 16 columns.

Rows and columns were represented by two sets of mutually orthogonal metallic strips, made of thin copper foil stuck on the support plastic leaf, with piezoresistive rubber (thickness 0.5 mm) installed between them, which created sensing cells in the points of crossing. Resistance of the cell with piezoresistive rubber changes as a function of pressure between the lower and the upper electrode (Fig.2.13). Individual sensor cells operated as resistive voltage dividers. Electronics circuits excited input rows and collected output columns signals. The outputs of the matrix are equipped with circuits providing power and impedance matching, the necessary interface for connection to a supervising PC via multi-function data acquisition card, which was used for the service of the array, measurement process control, signal and data processing [38].

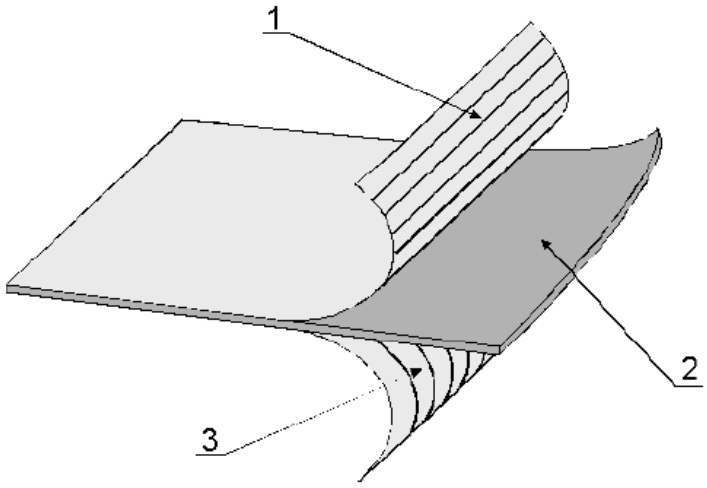

Figure 2.13 MTS with piezoresistive material between electrodes [38]
1- top electrodes 2- piezoresistive material 3- bottom electrodes.

The operation principle of the MTSA is shown in Fig. 2.14. In the presented construction electrodes were located on both sides of the piezoresistive layer. Conductivity of the material between electrodes in a sensor cell depended on the local force or pressure. Variations of the sensor cells volume conductivities were measured in normal direction to the MTSA plane.

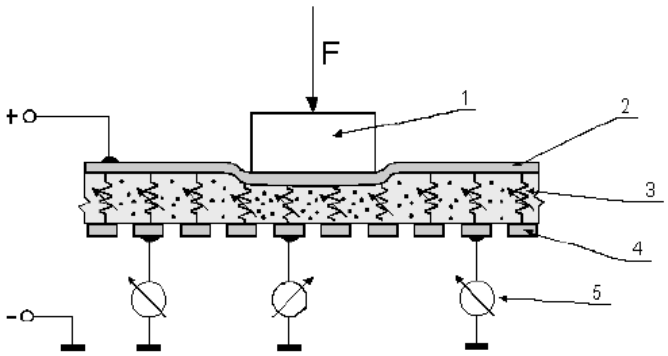

Figure 2.14 Piezoresistive principle of MTS with measurement current fluctuation [38]. 1- charging 2- the top foil with electrodes 3- piezoresistive material 4- the bottom foil with electrodes 5- measuring devices.

Since the direct measurement of conductivity is rather complicated, an indirect measurement method was used with measurement of resistance divider voltage on the output leads. An equivalent circuit of the sensor array resistor network is shown in Fig. 2.15.

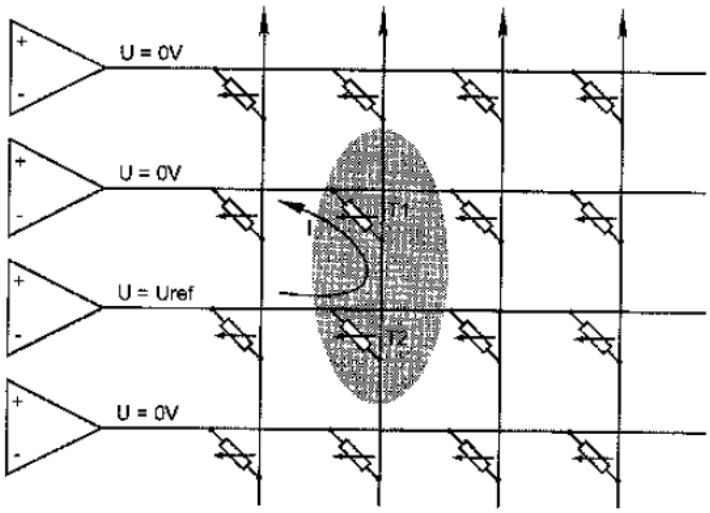

Figure 2.15 Equivalent circuit of the piezoresistive matrix sensor [38].

In Figure 2.15, all tactile cells were connected together, and therefore significant resistor change in the network could be detected. The electronic circuit could partially reduce the cross-talk by the zero-voltage-method. The resistance-to-pressure characteristic of the piezoresistive material is not linear (Figure 2.16). Sensitivity is very high in the small pressure range mainly (about 20 Ω/Pa at the pressure level of 10 kPa). The Full scale

resistance change is from 500 MΩ to 100 Ω (Fig. 2.16). the output obtained from the sensor is shown in Figure 2.17.a and Figure 2.17.b. Peak points correspond to contact points. Z axis shows the resistance change.

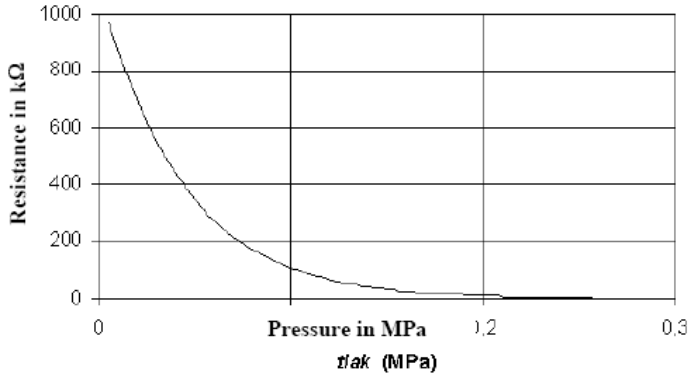

Figure 2.16 Resistance-to-pressure characteristic of the piezoresistive material [38].

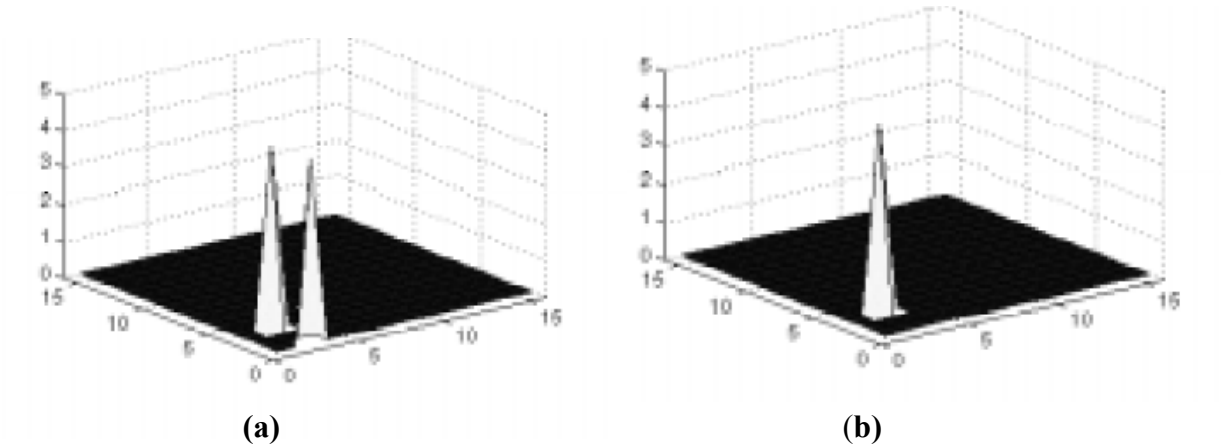

Figure 2.17 a) The output of the piezoresistive tactile sensor for two contact points **b)** The output of the piezoresistive tactile sensor for one contact point [38].

3. METHODS

3.1 Basic Design Principles

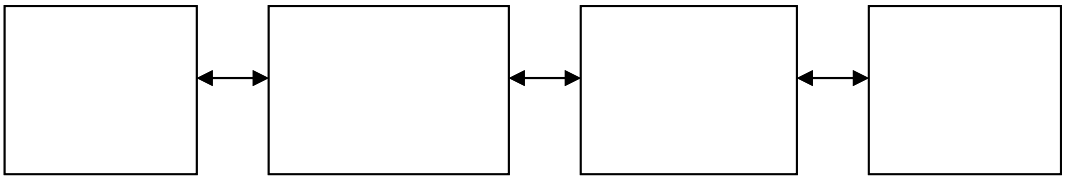

Figure 3.1 Block diagram of the tactile sensor system.

The electronics design of my thesis consists of four parts: optical array sensor, control unit, data acquisition card and computer (Fig. 3.1). The voltage outputs of the sensor are selected via control unit and read by data acquisition card through computer and Matlab.

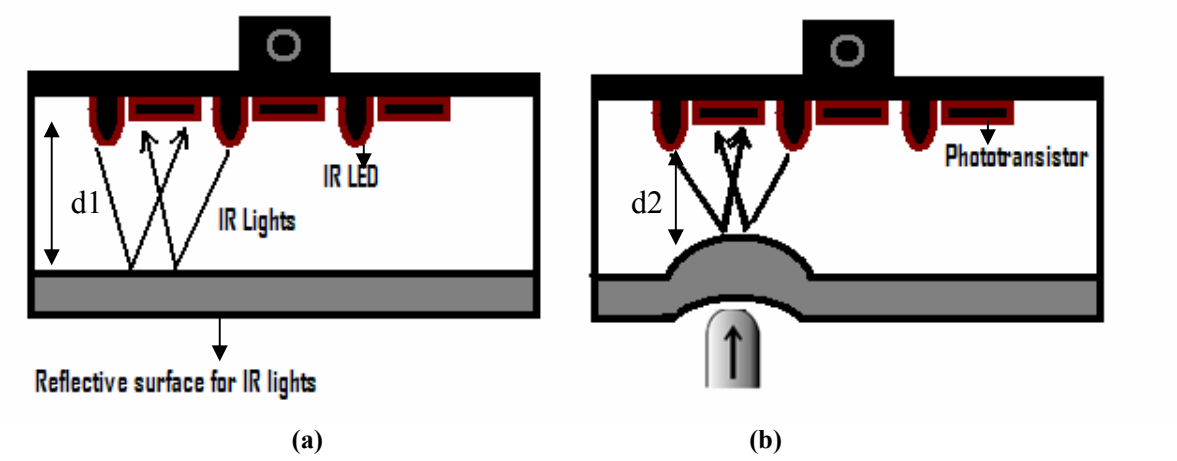

Figure 3.2 Working principle of the sensor a) un-deformed surface, b) deformed surface.

The emitted IR lights reflect from the silicone rubber surface and detected by phototransistors (Fig. 3.2.a). When an object contacts to the surface, the surface deforms (Fig 3.2.b) and the distance between surface and phototransistors gets smaller (d2<d1). This increases intensity of the light on the phototransistor.

3.2 Hardware

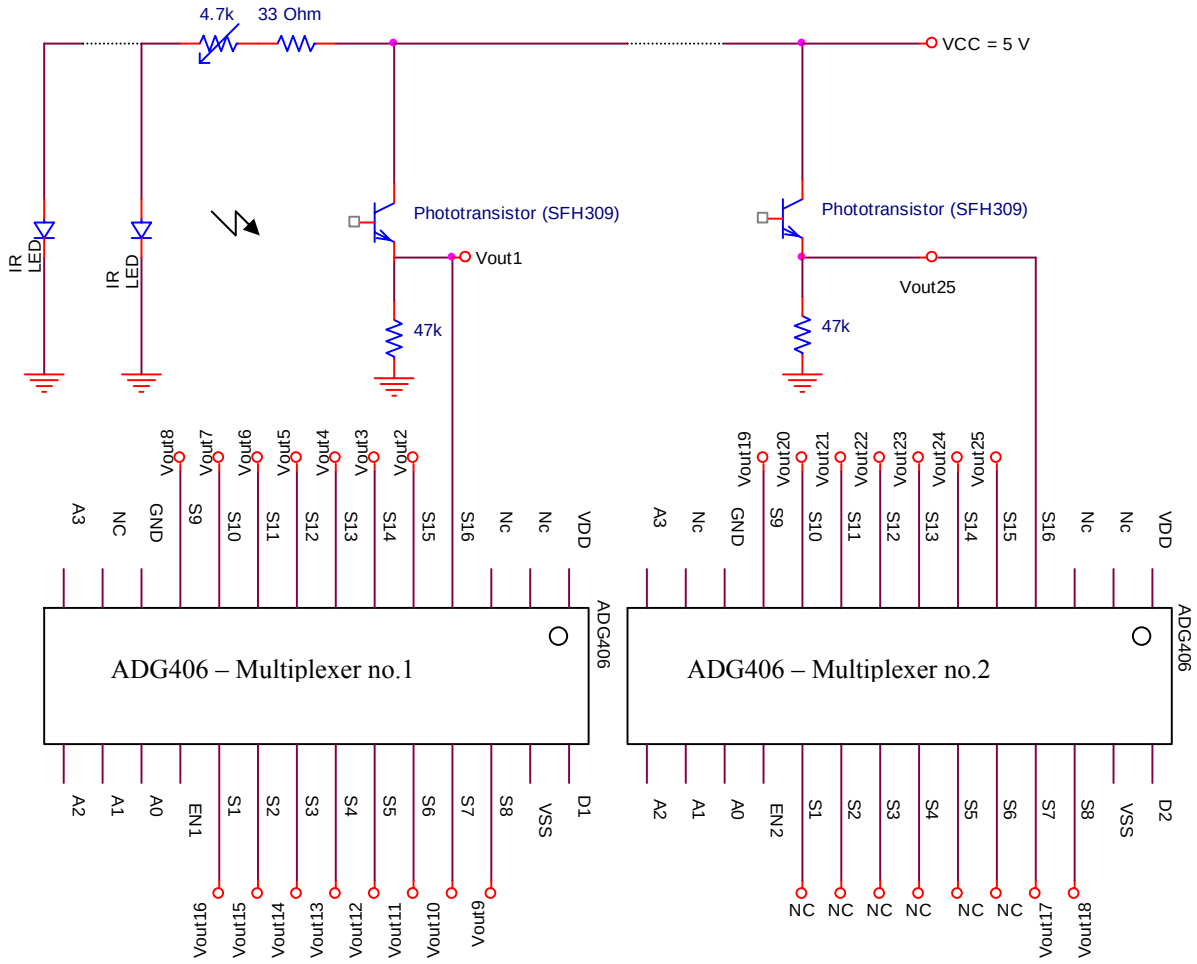

Figure 3.3 Circuit schematic of the system.

The electronics design is powered by a commercial 5V / 300 mA direct current power supply (not shown). All circuits use low-power components to minimize energy consumption. The nominal current requirement of the device is 40 mA.

The 33 Ω resistance was used to protect the circuit from high current when the potentiometer (4.7 k Ω) was set to zero by the user. The maximum current is about 150 mA and this does not damage to the circuit. The potentiometer varies the light output and this changes the sensitivity of the sensor.

The circuit diagram of the optical tactile array sensor is shown in Fig. 3.3. 16 IR-LEDs and 25 photodiodes were used but just first and last elements of the IR-Leds and photodiodes were shown.

Phototransistors (SFH 390) are sensitive to IR lights and the emitter voltage across the resistor will be high with incident lights, and in dark conditions the output will be nearly zero.

SFH 309 phototransistor has also an IR filter on the surface so that light with a limited range of wavelengths could pass. Phototransistor is most sensitive to 900 nm wavelength (Fig. 3.4)

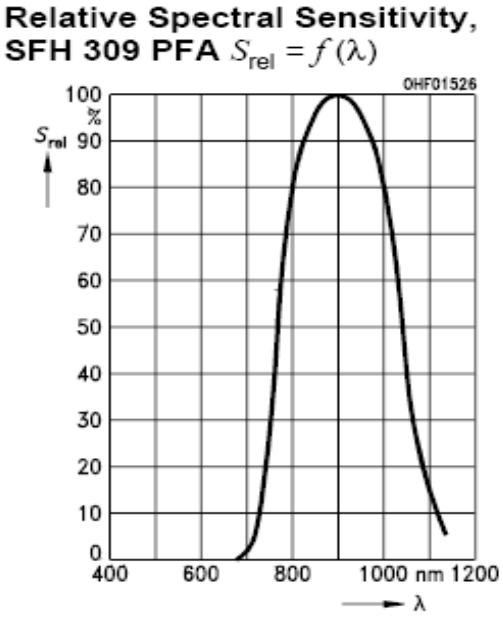

Figure 3.4 Spectral sensitivity of phototransistor.

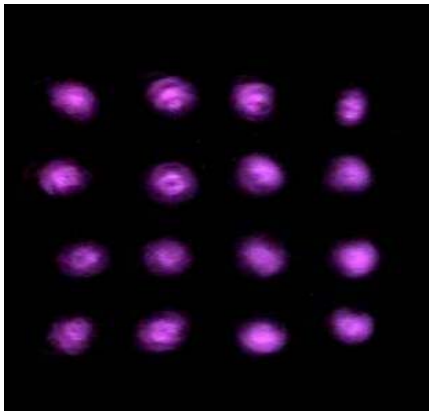

Figure 3.5 Camera image of the array IR LEDs captured during operation.

In the Fig 3.5, a camera image of the sensor is shown during normal operation. This image was captured by an IR sensitive camera and Kodak IR filter (800-1000 nm).

The optical tactile array sensor consists of 25 parts of optical sensing elements as a 5x5 array. The optical sensing elements are phototransistors which are sensitive to infra-red light. Each element was soldered on a circuit board and IR (Infra Red) LEDs were soldered between photodiodes in a 4x4 array. Each phototransistor is located 0.5 cm away from each other and the sensor has 2.5x2.5 cm active area (Figure 3.6).

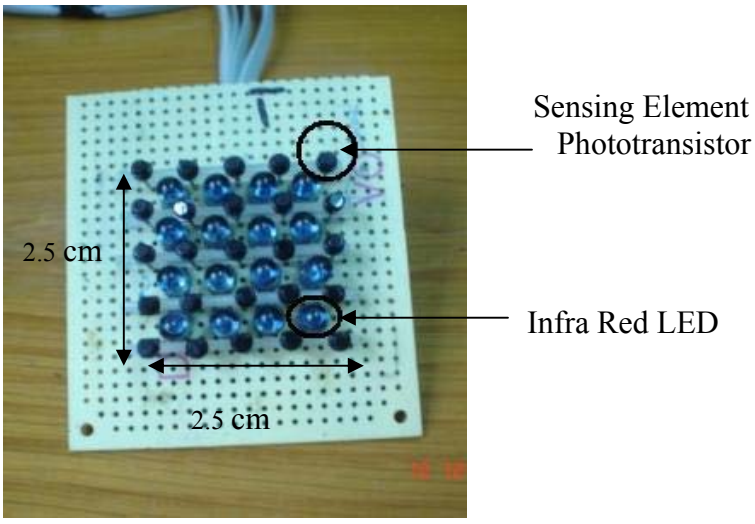

Figure 3.6 The 5x5 Optical tactile array sensor.

After completing circuit boards of the tactile sensor array and housing in an aluminum case and facing with the silicone rubber touch surface, the output of the sensors was connected with the control unit. The control unit is composed of two multiplexers (ADG406) to select the voltage output of the 25 phototransistors one by one. The multiplexes were controlled with a National Instrument Data Acquisition Card PCI-Mio 16e-1.

ADG406 Multiplexers are powered by single supplies and can work with 5V direct-current. They each have 16 channels and have fast switching on/off times. Fast switching enables near-real time data acquisition 16 voltage outputs were connected to the multiplexer 1 and the other 9 outputs were connected with multiplexer no. 2 (Fig. 3.1).

By setting enable pins (EN no. 1 and EN no. 2 in Fig. 3.3), high or low condition of the multiplexer was set for operation. The multiplexers were connected in parallel. Each multiplexer has 5 control bits including “enable” option. A0-A3 are control bits and by changing their conditions (on-off) voltage output of the specified sensor (Vout1 – Vout 25) was selected according to the truth table of ADG406 given by manufacturer.

Data output from multiplexers (D) were read by two analog input channels (ACHO-ACH1) of the data acquisition card. 6 digital outputs of the data acquisition card (DIO-DI5) were connected to (EN1, EN2, A0-A3) (not shown in Fig. 3.3). Data selection circuit was enclosed in a metal case and flexible connection cables were arranged (Fig. 3.9).

After soldering the photodiodes and infrared LEDs to the circuit board enclosed with an aluminum case of 5.6cm x 5.6cm 3cm (Fig. 3.7.a, Fig. 3.7.b).

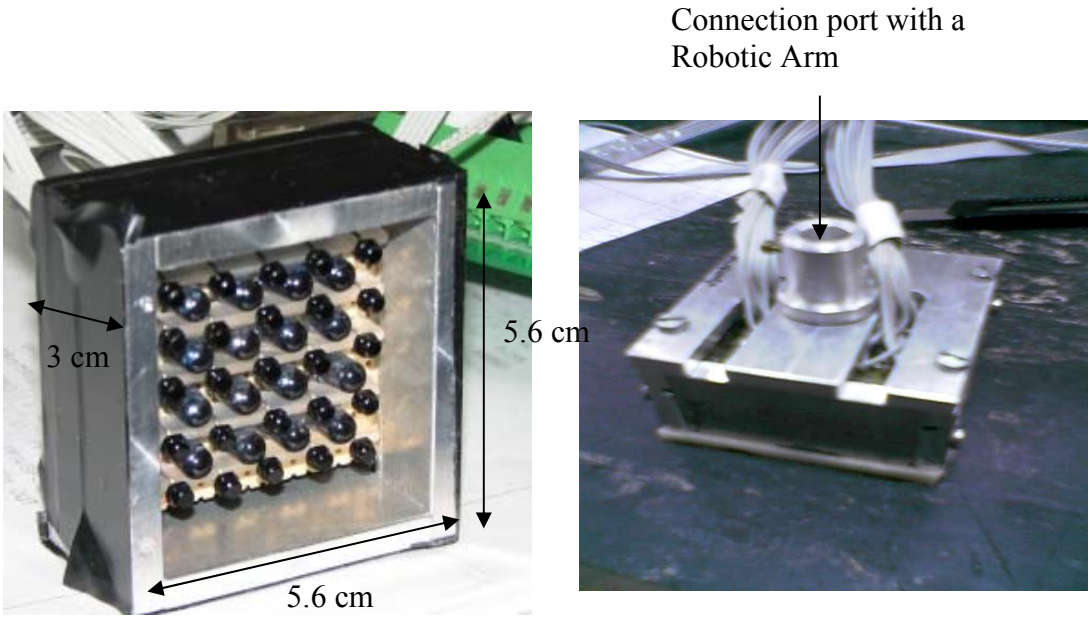

Figure 3.7 a) Tactile sensor in an aluminum case (front view) **b)** Tactile Sensor in an aluminum case (back view).

As a tactile surface, Smooth-Sil 910 silicone rubber was used, because it is non-toxic and biocompatible. It has high tear strength, and easy to modify to obtain various degrees of softness. It has two components: silicone rubber and chemical mixture. By mixing different ration of two components, it is possible to arrange the level of softness. The surface of the tactile sensor must be soft and compatible with tissue and also does not harm to the sample when it is touched. When it was cut, any air bubble was seen in the phantom.

According to instructions given with the Smooth-Sil 910, I used 1/10 mixture of two components to mold the silicone rubber surface. In our applications, 3 g / 33 g was arranged and molded into a plastic case. The prepared silicone rubber faced with metal case of the sensor by strong adhesives (Fig. 3.8).

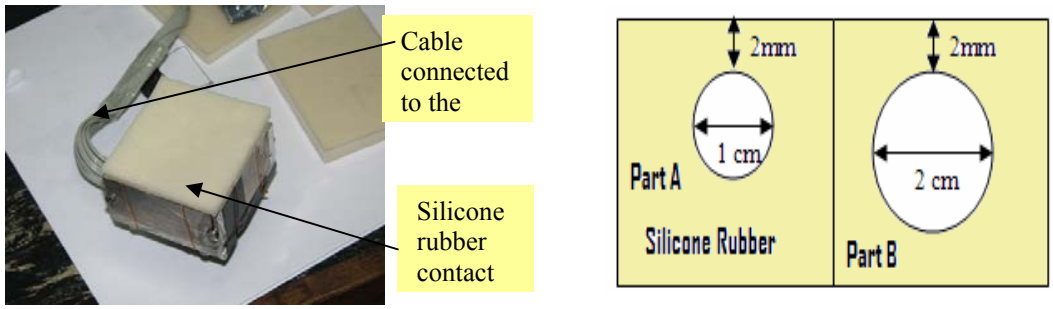

Figure 3.8 a) Silicone rubber placed on the tactile sensor **b)** Phantom no.1 (Part A) and Phantom no.2 (Part B).

While preparing phantoms that may simulate breast and lesion, the ratio was about 1/5 to have softer silicone rubber than sensor's touch surface. Thus, we could have the proper softness and could put 1 and 2 cm diameter spherical objects in them (Fig. 3.8.b). The objects have been placed just 2 mm under the silicon rubber. The touch surface of the optical tactile array sensor and phantoms were made from the same silicone rubber but their softness is not the same because of the ratio of two components.

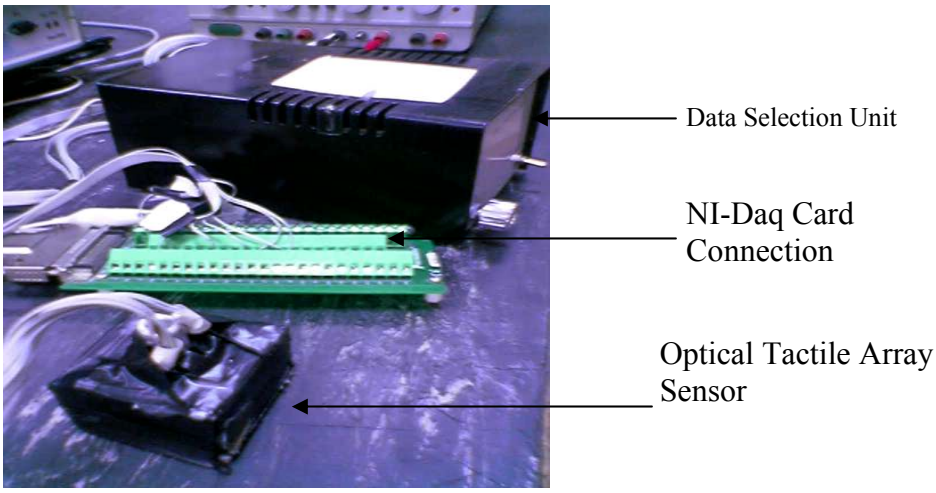

Figure 3.9 Connections between control unit, tactile array sensor and DAQ card.

Figure 3.9 shows the all three parts of the sensor: tactile sensor array, control unit and data acquisition card.

3.3 Calibration

To calibrate the optical tactile array sensor, Von Frey Hairs (VFHs) were used. VFH is an element which has a plastic indenter. The indenter is calibrated to a specific force (180g in Fig. 3.10.c). Each one of them was touched to the dotted part (not shown) of the tactile sensor's elastic surface, which was made of silicone rubber, to see the response and have the calibration curves to understand its working characteristics.

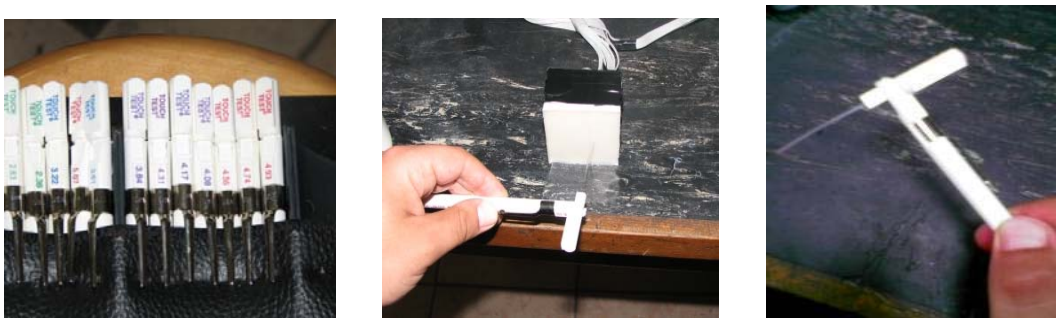

(a) **(b)** **(c)**

Figure 3.10 a) VFHs with different grams **b)** Calibration data acquisition by using VFH **c)** a VFH of 180 g.

Each square on the Fig. 3.11 corresponds to a sensing element of the optical tactile array sensor. By using different grams of VFH (10, 15, 25, 60, 100, 180, 300), the dotted parts of the tactile sensor were touched and at the time touching, the voltage values of interest were recorded. Using voltage outputs, grams versus voltages were graphed and linear curve fitting was applied using Microsoft Excel.

	1	2	3	4	5
1	ch5	ch4	ch3	ch2	ch1
2	ch6	ch7	ch8	ch9	ch10
3	ch15	ch14	ch13	ch12	ch11
4	ch16	ch17	ch18	ch19	ch20
5	ch25	ch24	ch23	ch22	ch21

Figure 3.11 Channel chart for the tactile array sensor.

Figure 3.11 shows the channel placement and their names according to data acquisition system. The results of the calibration were tabulated and the working characteristic of each phototransistor of the tactile sensor was determined. The voltage output of phototransistor 1 is depicted as “ch1” and voltage output 25 is called “ch25” in Fig. 3.11.

By using aesthesiometer which is an adjustable two touch point tester (aesthesiometer), we can test the ability of discrimination of our optical tactile sensor array. The aesthesiometer was adjusted to 0.5, 1 and 1.5 cm and touched to the surface of the sensor as seen in the Figure 3.12 below.

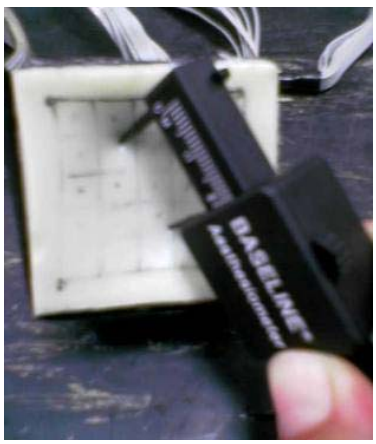

Figure 3.12 Aesthesiometer.

3.4 Software

The control software for the presented device was written in Matlab (version 6.5, The Math Works) to control digital control bits of the multiplexers and to acquire analog outputs of the sensors with two analog input channels of the data acquisition card.

After the program is launched with MATLAB software, calibration needs to be performed. After calibration, the data acquisition program can provide a map of the tactile sensor. The main data acquisition program is called “realtime.m”. First of all, the settings are performed.

```
ai=analoginput('nidaq',1); % assigns the names of the analog inputs
ch=addchannel(ai,0:1);     % assigns two analog channels to acquire
```

Analog inputs are connected with the data output pins of the two multiplexers.

Sampling rate, input type, trigger type and samples per trigger were assigned as below.

```
ai.SampleRate=100000;
ai.SamplesPerTrigger=10;
ai.TriggerType='Immediate';
ai.InputType = 'SingleEnded';
```

Even though the sampling rate was 100000 in the program, the actual sampling rate 10 of all data acquisition process. Because program was able to have all datum from 25 phototransistors took about 0.1 seconds. To optimize the time, I did not write sub-programs and functions not to reduce the time.

Multiplexers were controlled by setting digital output channels of the NI Data acquisition Card.

```
%digital  out channels adjustment
dio=digitalio('nidaq');    %assigns digital outputs
addline(dio, 0:7, 'out');  %assigns 8 bits digital outputs
```

By using “addline” command, 8 digital outputs were introduced.

```
pval=[0 0 0 0 0 0 0 0 ];
putvalue(dio,pval);      % resets the digital outputs
```

“putvalue” command puts the value of “pval” to the digital outputs of the data acquisition card.

```
pval=[ 0 0 0 0 1 1 0 0 ]; % puts the number to the digital output
putvalue(dio,pval);
start(ai);                %starts data acquisition
data=getdata(ai);
data=max(data);
ch1=data(1);
ch17=data(2);
```

“*start*” command starts the data acquisition and “getdata” gives the acquired data. Now that the program uses two analog inputs, it gives two outputs. The first data gives the output voltage from multiplexer 1 and the other gives data from multiplexer 2.

At firs run of the *realtime.m*, calibration matrix is obtained and this matrix will be subtracted each time from the new data. By this way, difference between data is imaged by Matlab and visual and quantitative measurements can be done.

```
clb= [ ch5 ch4 ch3 ch2 ch1;              % calibration matrix
       ch6 ch7 ch8 ch9 ch10;
       ch15 ch14 ch13 ch12 ch11;
       ch16 ch17 ch18 ch19 ch20;
       ch25 ch24 ch23 ch22 ch21];
```

The resultant image is found as:

```
diff=(clb-map);
        gain=30;
        image(gain*diff);
```

“*diff*” matrix is mapped and this is the output of the other *.m files* for further modification and evaluation of data.

3.5 Analysis

3.5.1 Filter

The "*diff*" matrix is the output of the main program "*realtime.m"*. The output is filtered using "*filter.m"*. The filtering finds peaks in the tactile image by thresholding. Since multiple sensor cells may be selected by thresholding local minima were eliminated by comparing the cells (see Appendix).

In the filter output, the local maxima were passed unaltered; the remaining cell outputs were set to zero.

If a data is the maximum of the *diff* matrix, it is depicted as *global maximum.*

th=0.5; % global threshold
th2=0.85; % local threshold
"th" is set as threshold that is 0.5xglobal maximum and "*th2*" as local threshold for neighbour pixels of the interested point.

mapx=diff; % change the mapx name with the target

```
   a= [1 1; 1 2;2 1;2 2]';
```

"*a*" shows the indices of neighbour of channel 1 (Fig. 3.11).

```
 [sa]=sub2ind([5 5],a(1:2:max(size(a))*2),a(2:2:max(size(a))*2))
       t=find(  (mapx(sa) >(max(max(mapx) )*th)) &( mapx(sa)>
max(mapx(sa))*th2 ))

       if isempty(t),
       mapx(sa)=0;
       else
           t1=setdiff([1:max(size(a))],t)
       mapx(sa(t1))=0;
       end
```

This program looks indices for maximum and global maximum, and set the pixel to zero if the value is smaller than threshold values.

3.5.2 Distance detection

After filtering the data and finding the peak values, the distance between of the peak were calculated with the distance.m file according to algorithm below;
"*diff*" is the output of the *filter.m* and the distance between peaks indiced by k,t is given as f(k,t).

```
% distance detection
mapx=diff;
 [i,j]=ind2sub([5 5],find(mapx>0))
for k=1:max(size(i))
for t=1:max(size(i))
    f(k,t)=norm([i(t) j(t)]-[i(k) j(k)])
end
end
```

This program finds the indices of the cells which are found by "*filter.m*" and finds the Euclidean distance between them. By multiplying the calculated distance with the sensor resolution (5 mm), the distance actual distance can be found.

3.5.3 Bicubic Interpolation

The "diff" matrix can be mapped as 5x5, but for visual enhancement bicubic interpolation is applied to the matrix. Bicubic interpolation is a method to do interpolation in two dimensions.

A function of two variables which has known values only at discrete points, can be approximated in between the discrete points using interpolation, and bicubic means that the interpolated surface is continuous everywhere and also continuous in the first derivative in all directions.

If the function values and the derivatives are known at the four corners (0,0), (1,0), (0,1), and (1,1) of the unit square, and the interpolated surface is

$$p(x,y) = \sum_{i=0}^{3}\sum_{j=0}^{3} a_{ij}x^i y^j \qquad (3.1)$$

The interpolation problem consists of determining the 16 coefficients a_{ij}. At the corner points, the derivative in the *x*-direction and the *y*-direction is needed, as well as the cross derivative *xy*.

3.5.4 Statistical analysis

For linearity tests, linear regression analysis was applied using Microsoft Excel. Best-fit equations and R^2 values were calculated. If the goodness of fit was higher than this threshold, the calibration was considered to be linear. R^2=0.9 was accepted as a threshold for a linear fit.

4. RESULTS

4.1 Calibration

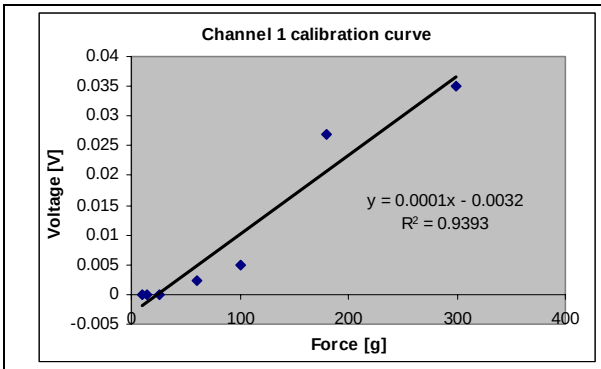

(a)

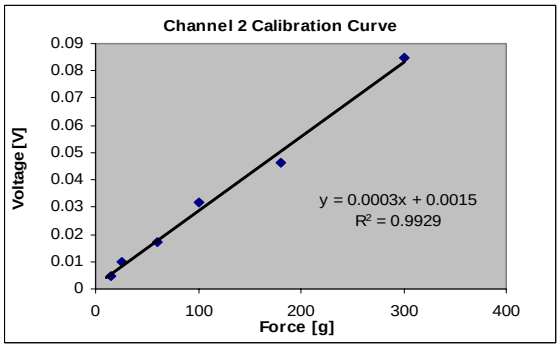

(b)

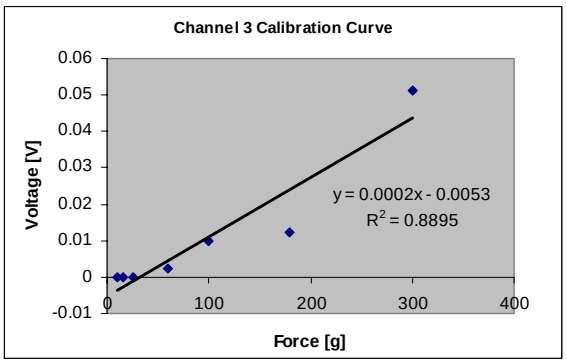

(c)

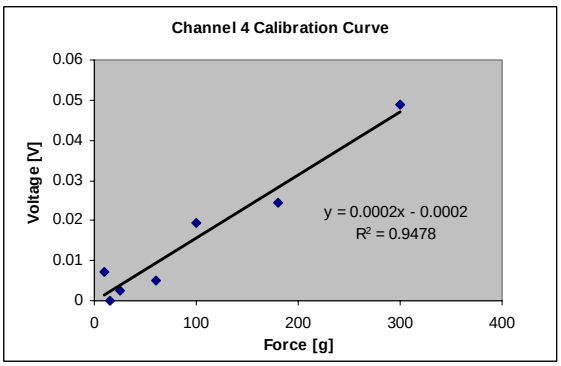

(d)

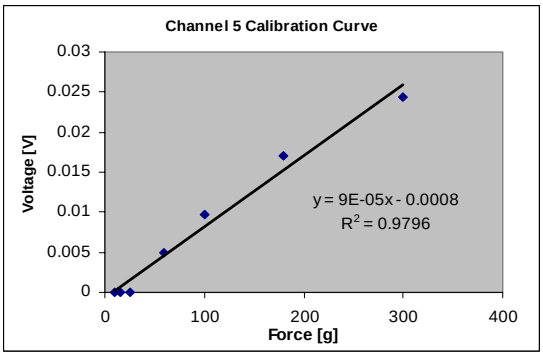

(e)

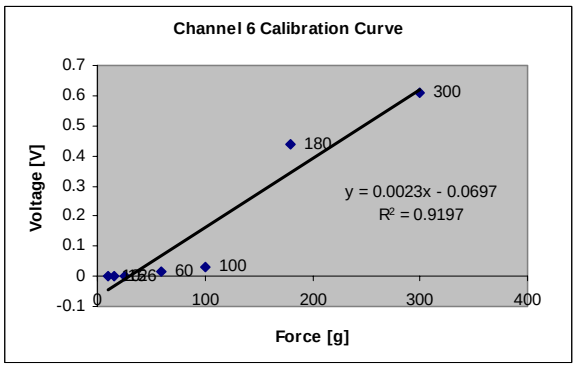

(f)

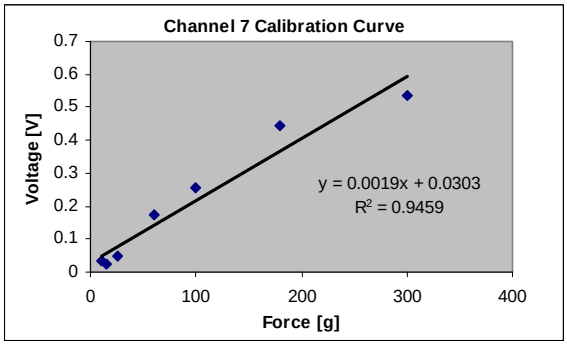
Channel 7 Calibration Curve
Voltage [V]
Force [g]
y = 0.0019x + 0.0303
R² = 0.9459

(g)

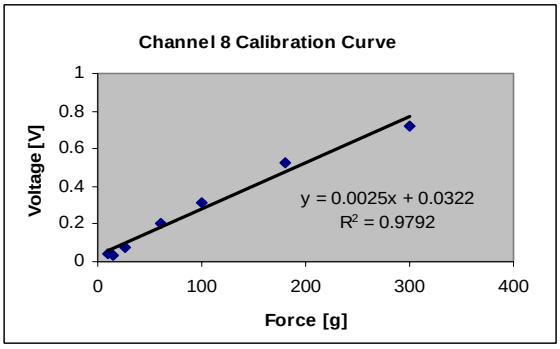
Channel 8 Calibration Curve
Voltage [V]
Force [g]
y = 0.0025x + 0.0322
R² = 0.9792

(h)

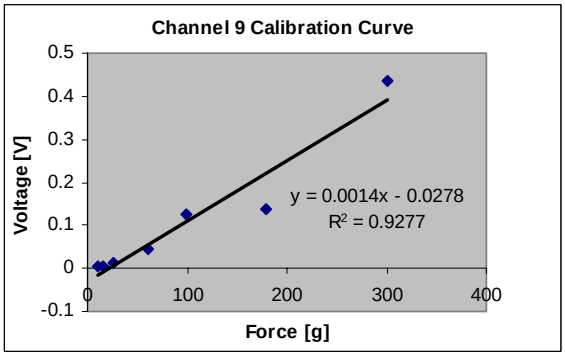
Channel 9 Calibration Curve
Voltage [V]
Force [g]
y = 0.0014x - 0.0278
R² = 0.9277

(i)

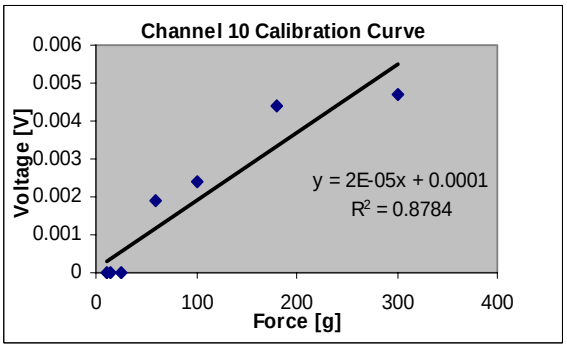
Channel 10 Calibration Curve
Voltage [V]
Force [g]
y = 2E-05x + 0.0001
R² = 0.8784

(j)

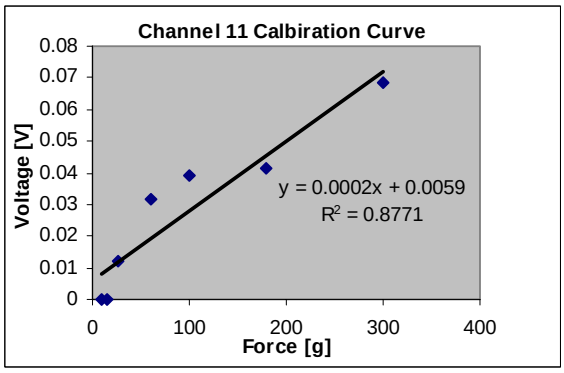
Channel 11 Calbiration Curve
Voltage [V]
Force [g]
y = 0.0002x + 0.0059
R² = 0.8771

(k)

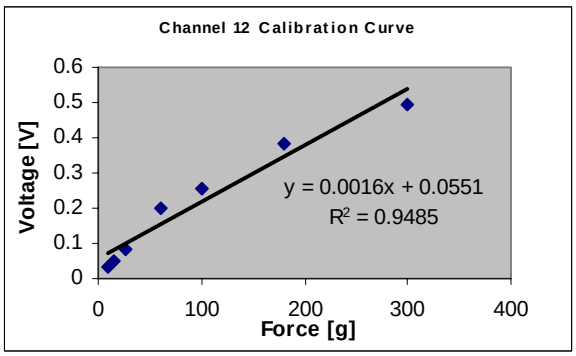
Channel 12 Calibration Curve
Voltage [V]
Force [g]
y = 0.0016x + 0.0551
R² = 0.9485

(l)

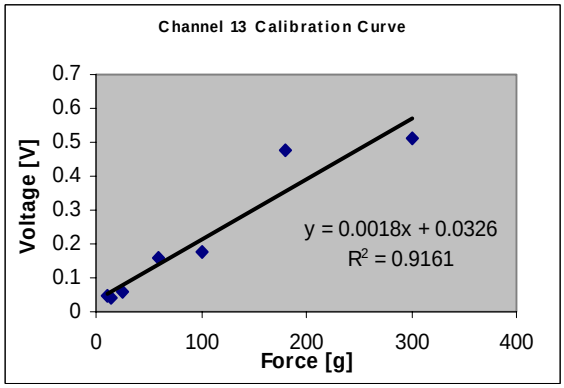
Channel 13 Calibration Curve
Voltage [V]
Force [g]
y = 0.0018x + 0.0326
R² = 0.9161

(m)

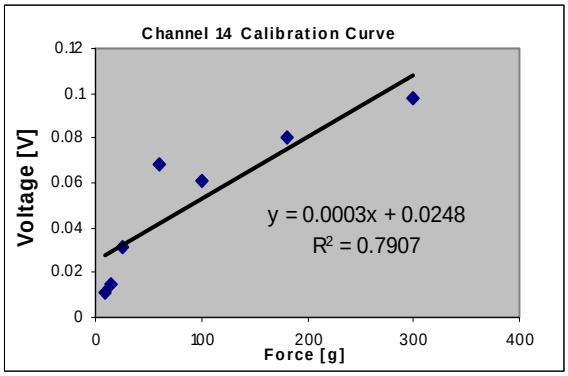
Channel 14 Calibration Curve
Voltage [V]
Force [g]
y = 0.0003x + 0.0248
R² = 0.7907

(n)

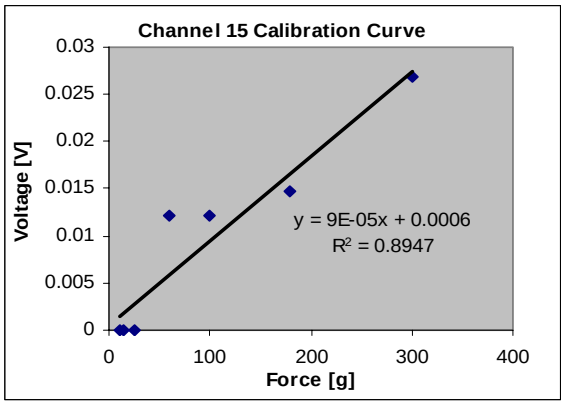
Channel 15 Calibration Curve
Voltage [V]
Force [g]
y = 9E-05x + 0.0006
R² = 0.8947

(o)

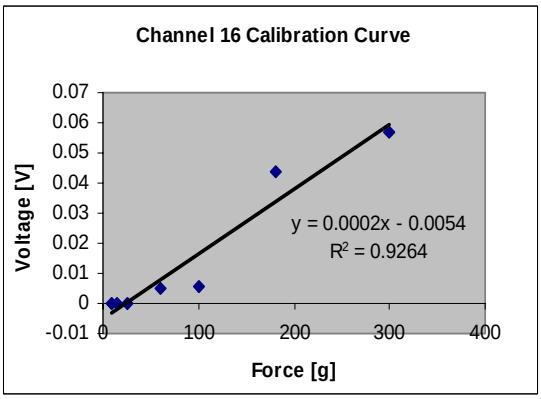
Channel 16 Calibration Curve
Voltage [V]
Force [g]
y = 0.0002x - 0.0054
R² = 0.9264

(p)

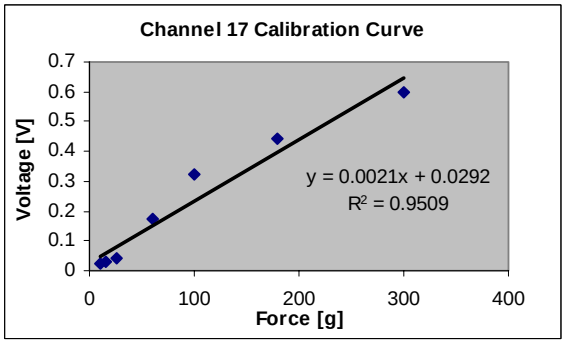
Channel 17 Calibration Curve
Voltage [V]
Force [g]
y = 0.0021x + 0.0292
R² = 0.9509

(q)

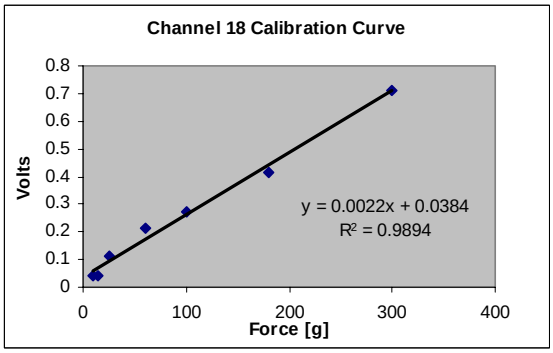
Channel 18 Calibration Curve
Volts
Force [g]
y = 0.0022x + 0.0384
R² = 0.9894

(r)

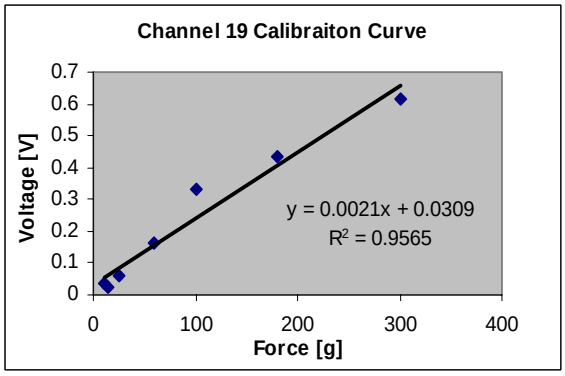
Channel 19 Calibraiton Curve
Voltage [V]
Force [g]
y = 0.0021x + 0.0309
R² = 0.9565

(s)

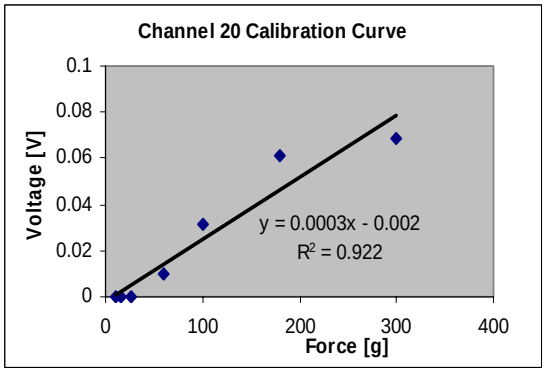
Channel 20 Calibration Curve
Voltage [V]
Force [g]
y = 0.0003x - 0.002
R² = 0.922

(t)

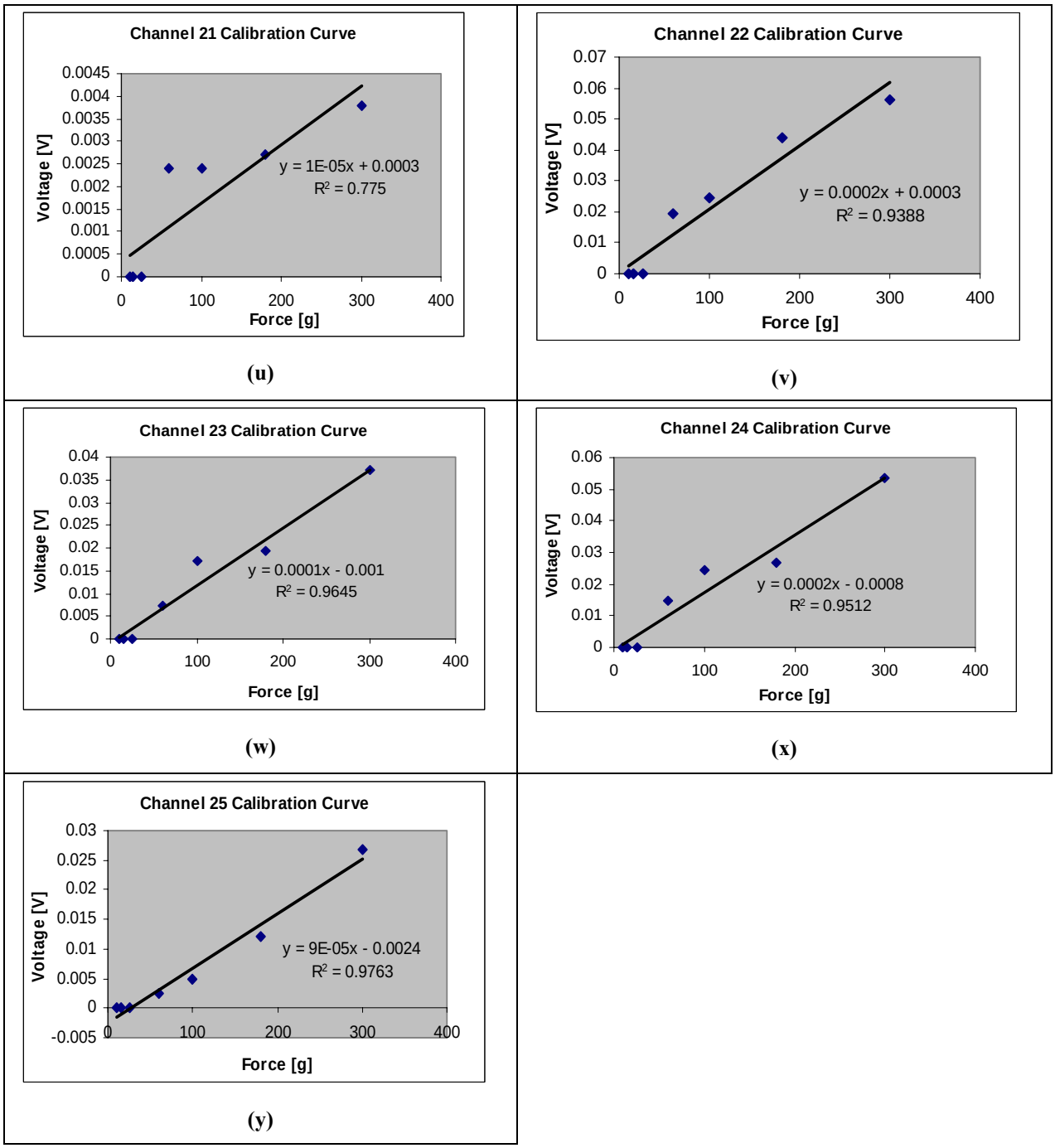

Figure 4.1 Force-Voltage calibration data of tactile sensor channels 1 - 25 corresponds to a - y respectively.

The calibration data is presented in Table 4.1. Most of the channels can be considered as linear. However, outputs of some channels (3, 10, 11, 14, 15, 21) deviated from best-fit lines and yielded low goodness of fit values.

4.2 Overall Performance Data

Table 4.1 Overall characteristic values of the sensor.

# of Channels	R^2	Sensitivity (slope)	Zero Error
1	0.9393	0.0001	-0.0032
2	0.9929	0.0003	0.0015
3	0.8895	0.0002	-0.0053
4	0.9478	0.0002	-0.0002
5	0.9796	9.00E-05	-0.0008
6	0.9197	0.0023	-0.0697
7	0.9459	0.0019	0.0303
8	0.9792	0.0025	0.0322
9	0.9277	0.0014	-0.0278
10	0.8784	2.00E-05	0.0001
11	0.8771	0.0002	0.0059
12	0.9485	0.0016	0.0551
13	0.9161	0.0018	0.0326
14	0.7907	0.0003	0.0248
15	0.8947	9.00E-05	0.0006
16	0.9264	0.0002	-0.0054
17	0.9509	0.0021	0.0292
18	0.9894	0.0022	0.0384
19	0.9565	0.0021	0.0309
20	0.922	0.0003	-0.002
21	0.775	1.00E-05	0.0003
22	0.9388	0.0002	0.0003
23	0.9645	0.0001	-0.001
24	0.9512	0.0002	-0.0008
25	0.9763	9.00E-05	-0.0024
Mean	**0.927124**	**0.00082**	**0.006544**

The average sensitivity of the sensor is 0.00082. The zero average zero error is 0.006544. According to the channel averaged data, the sensor output can be represented as;

$$y=0.0082X+0.0065444 \quad (4.1)$$

4.3 Phantom Experiments

Figure 4.1 shows the raw data when the sensor was applied on Phantom 1. The light area depicts the place on the object in Phantom 1. Figure 4.2 is the bicubic interpolation of the raw data for further data visualization. The filtering analysis located the suspicious lesion at coordinates (channel 14, 17, 18). According to the calibration, this lesion excreted maximum 208 gram force on the sensor on the sensor (channel17).

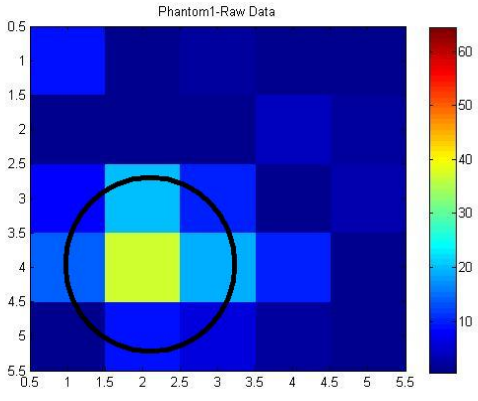

Figure 4.2 Raw data of the tactile sensor from phantom no.1.

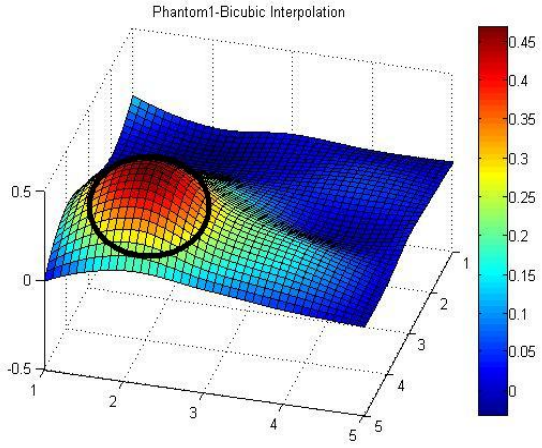

Figure 4.3 Results from phantom no.1 after bicubic interpolation.

The peak location of the output gives to the location of the hard object in phantom 1. Circled areas are regions of interest. In Fig. 4.1 raw data acquired by "*realtime.m"* is shown, and in Fig. 4.2 circled area shows the region of interest.

Figure 4.3 shows the output of the tactile sensor applied on phantom. Light areas are the locations of hard object in the Phantom no. 2.

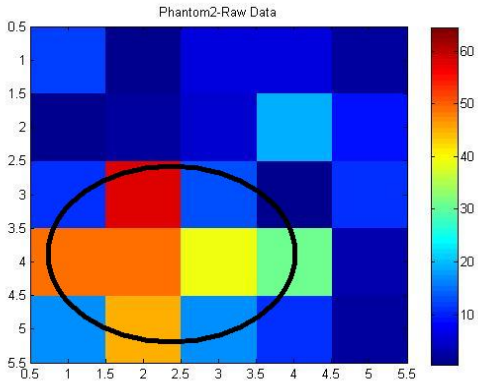

Figure 4.4 Raw data of the tactile sensor from phantom no.2.

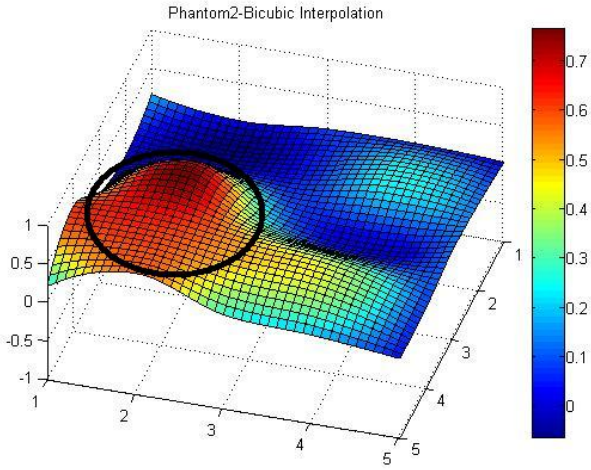

Figure 4.5 Bicubic interpolation of tactile sensor map for phantom no.2.

Circled areas depict the location of hard object in phantom no. 2. The raw data was the output of the "*realtime.m"* and was filtered by "*filter.m"*.

Quantitative measurement and comparison of two images**:**

Beyond the visual information about the lesion in the soft tissue, we need also quantitative comparison. By using an appropriate filter to find the suspected lesion, the Matlab program can calculate the area of region of interest.

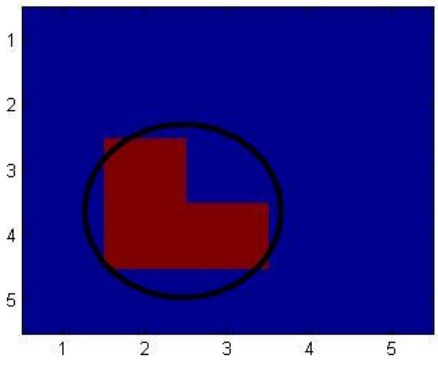

Figure 4.6 Filtered data of phantom no. 1.

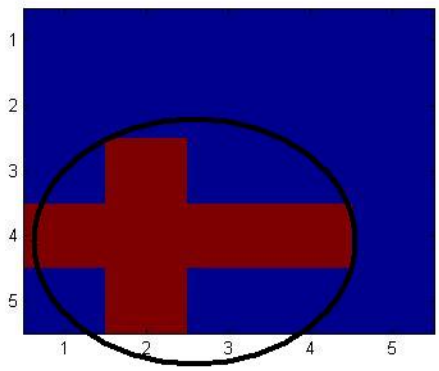

Figure 4.7 Filtered data of phantom no. 2.

As it is seen in Fig. 4.5, 3 pixels are above the threshold and the indices are calculated. For phantom 1, we have 3 indices (8, 9, 14) and for phantom 2 we have 6 pixels above the threshold (4, 8, 9, 14, 19) Fig. 4.6.

For the first phantom, the program filter.m gives that the pixels 8,9 and 14 are the suspicious regions. And for the second phantom, the program gives that the pixels 4, 8, 9, 10, 14 and 19 are the suspicious regions.

4.4 Experiments with different stimulus intensities

4.4.1 Stimulus: 300 g

In this test, a 300 gram Von Frey Hair was pressed on a certain part of the tactile sensor to see whether the tactile sensor was able to detect the contact point. In Figure 4.7.a the raw data is shown, and Figure 4.7.b bicubic interpolation of the raw data. The light areas depict the contact point by 300g VFH.

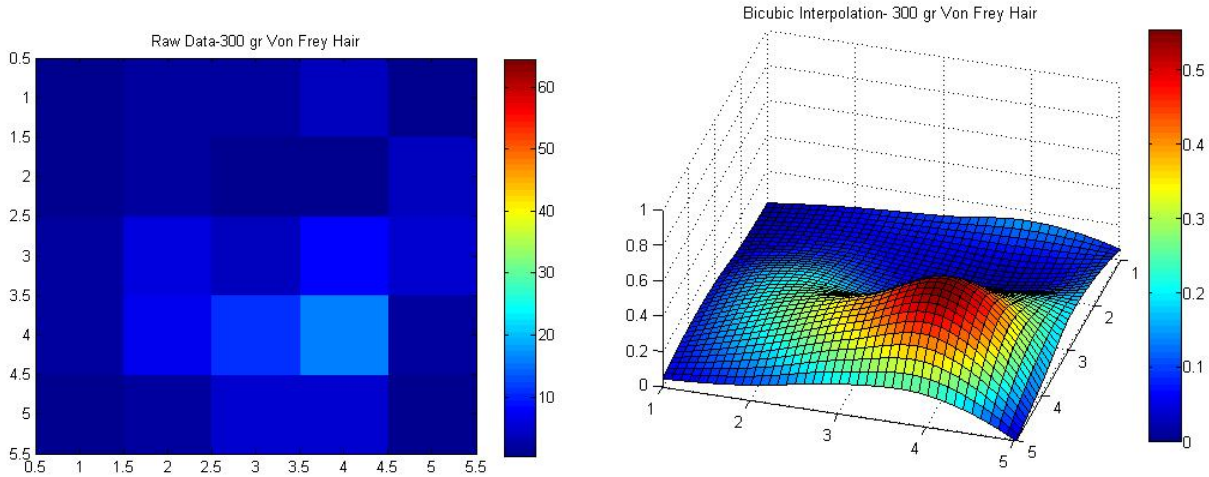

(a) **(b)**

Figure 4.8 a) Raw data after stimulating with 300 g VFH **b)** Bicubic interpolation of data after stimulating 300gr VFH.

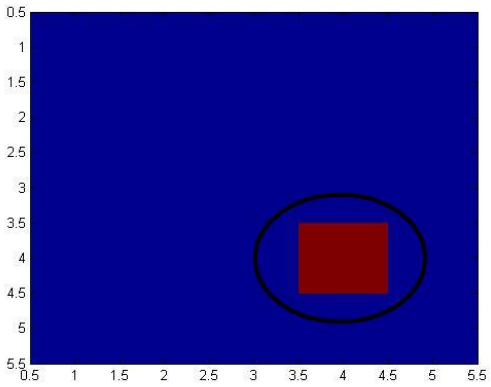

Figure 4.9 Filtered data after stimulating with 300 g VFH.

After filtering the raw data with *filter.m* (Fig. 4.8), indices of the peak point is found and channel number is determined. By using the calibration curves for that channel the contact force was predicted. The output (channel 19) was 0.542 Volts and this corresponds to 243.5 gram-force.

4.4.2 Stimulus: 180 g

In this test, a 180 gram Von Frey Hair was pressed on a certain part of the tactile sensor to see whether the tactile sensor was able to detect the contact point. The light areas depicts the location of contact. In Figure 4.9.a, the raw data is shown, and Figure 4.9.b is bicubic interpolated version of raw data for more convenient data visualization.

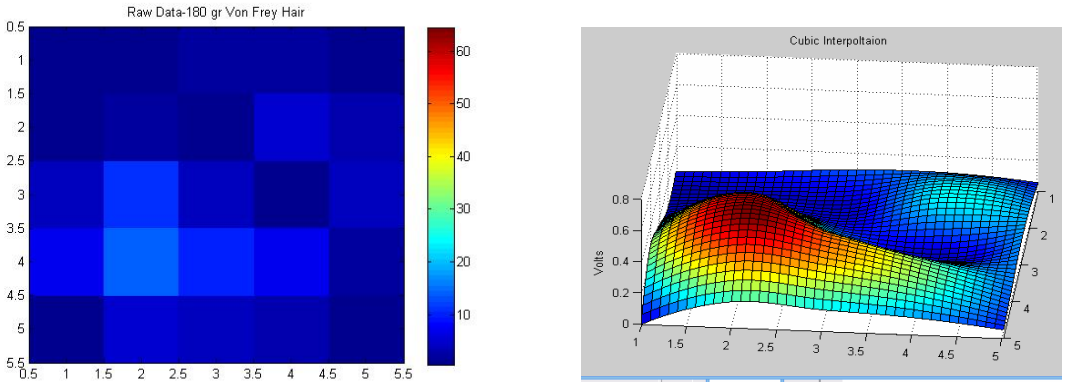

(a) **(b)**

Figure 4.10 a) Raw data after stimulating with 180 g VFH **b)** Bicubic interpolation of data after stimulating with 180 g VFH.

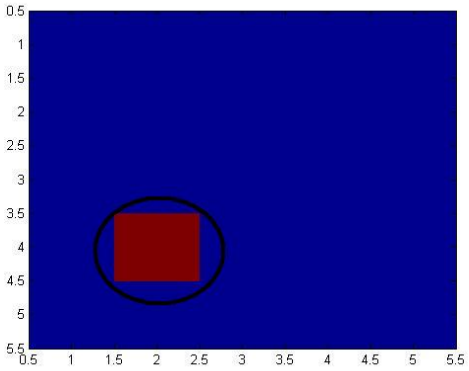

Figure 4.11 Filtered data after stimulating with 180 g VFH.

After filtering the raw data (Fig. 4.10) the peak value of the raw data was detected 0.4689 volts. And from the indices of the peak, the channel number was found. From the calibration equation, the force was calculated as 209 g-force.

4.4.3 Stimulus: 100 g

In this test, a 100 gram Von Frey Hair was pressed on a certain part of the tactile sensor to see whether the tactile sensor was able to detect the touch point. In Figure 4.11.a, the raw data is shown, and Figure 4.11.b is bicubic interpolated of raw data for more convenient data visualization.

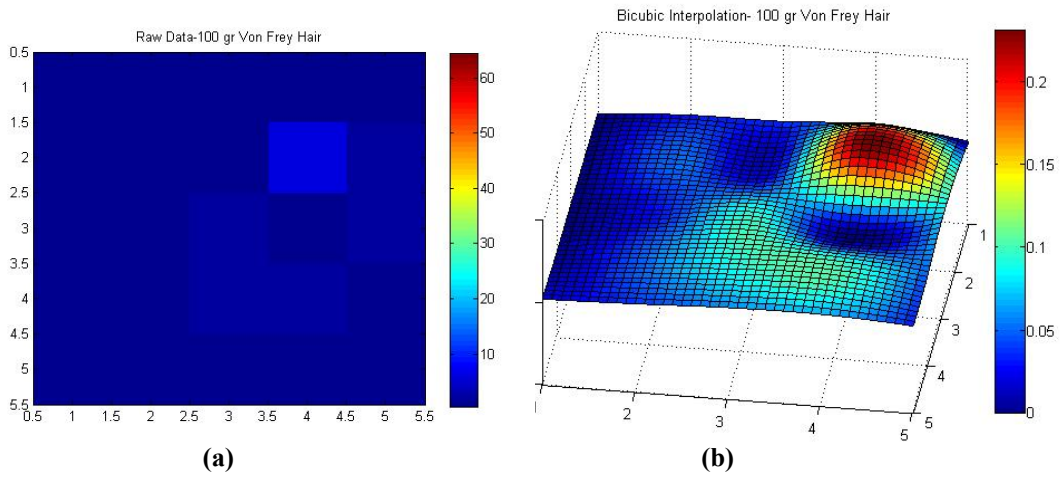

Figure 4.12 a) Raw data after stimulating with 100 g VFH **b)** Bicubic interpolation of data after stimulating with 100 g VFH

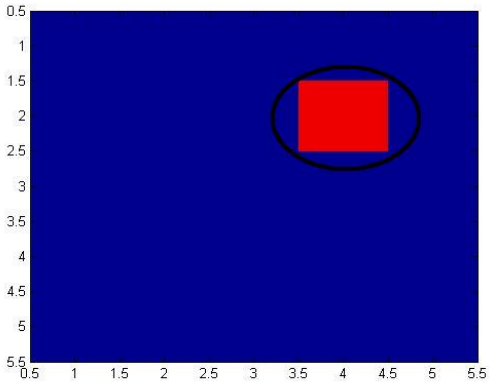

Figure 4.13 Filtered data after stimulating with 100 g VFH.

Circled area depicts the location of contact point (Fig. 4.12). After filtering the raw data, the peak point was detected as 0.2295 Volts (Channel 9). From the indices of peak data, the channel was found and calibration equation was used to calculate the force. This force was detected as 183 g-force.

4.4.4 Stimulus: 15 g

In this test, a 15 gram Von Frey Hair was pressed on a certain part of the tactile sensor to see whether the tactile sensor was able to detect the touch point. The light areas depict the contact point. In Figure 4.13a, the raw data is shown, and Figure 4.13.b is bicubic interpolated version of raw data for more convenient data visualization.

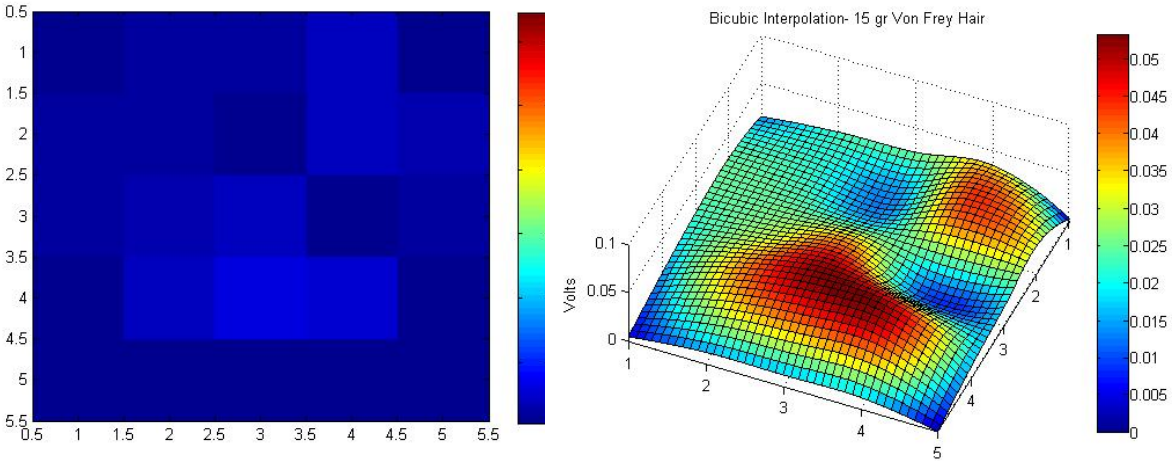

(a) **(b)**

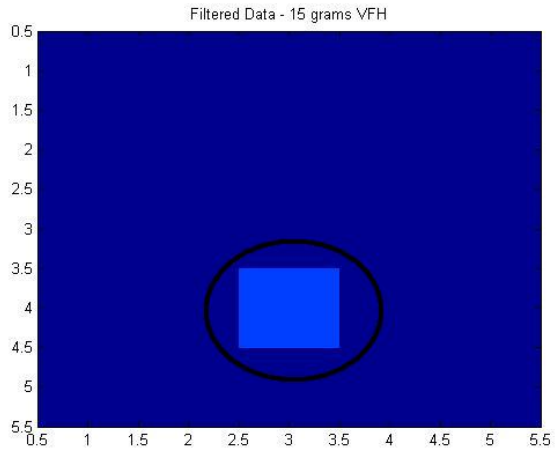

(c)

Figure 4.14 a) Raw data after stimulating with 15 g VFH **b)** Bicubic interpolation of data after stimulating with 15 g VFH **c)** Filtered data after stimulating with 15 g VFH.

After running the *filter.m* file, the indices of peak data and the number of channel was detected. From the calibration equation, the applied force was calculated as about 5.87 g-force.

4.5 Two-point discrimination experiments

4.5.1 Discrimination of stimuli spaced 0.5 cm apart

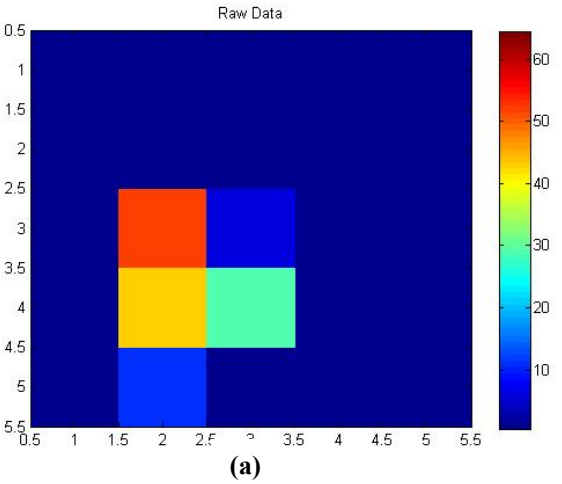

(a)

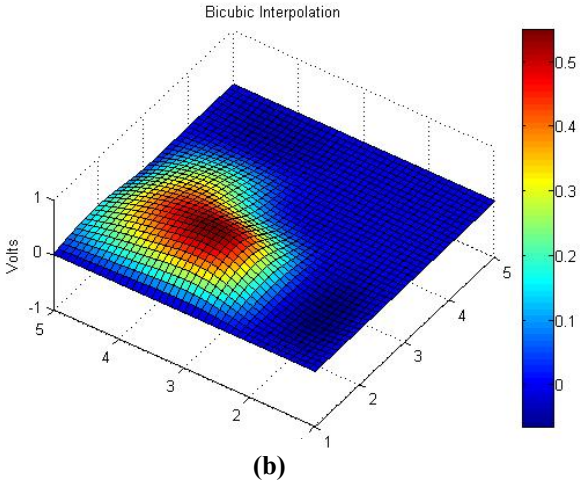

(b)

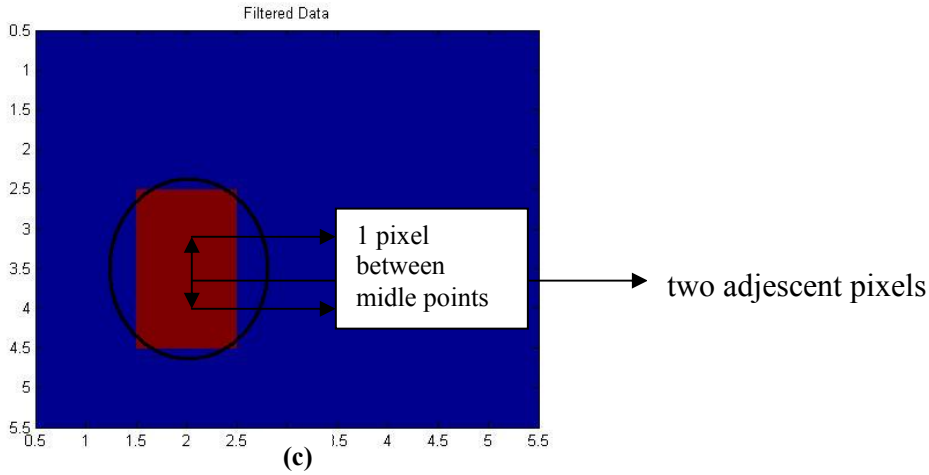

Figure 4.15 a) Raw data after stimulating two points for detecting distance btw. stimuli (0.5 cm) **b)** Bicubic interpolation of data after stimulating two points for detecting distance btw. stimuli (0.5 cm) **c)** Filtered data for detecting distance between stimuli (0.5 cm).

If we assume that there were 2 suspicious point and use "distance.m" the distance was found as 1 pixel. This corresponds to 0.5 cm (Fig. 4.14.c).

4.5.2 Discrimination of stimuli spaced 1 cm apart

In this experiment, the aesthesiometer was adjusted to 1 cm and applied to the tactile surface. In the Figure 4.15.a the raw data is presented and in Figure 4.15.b, the bicubic interpolation was performed for enhancing the tactile image.

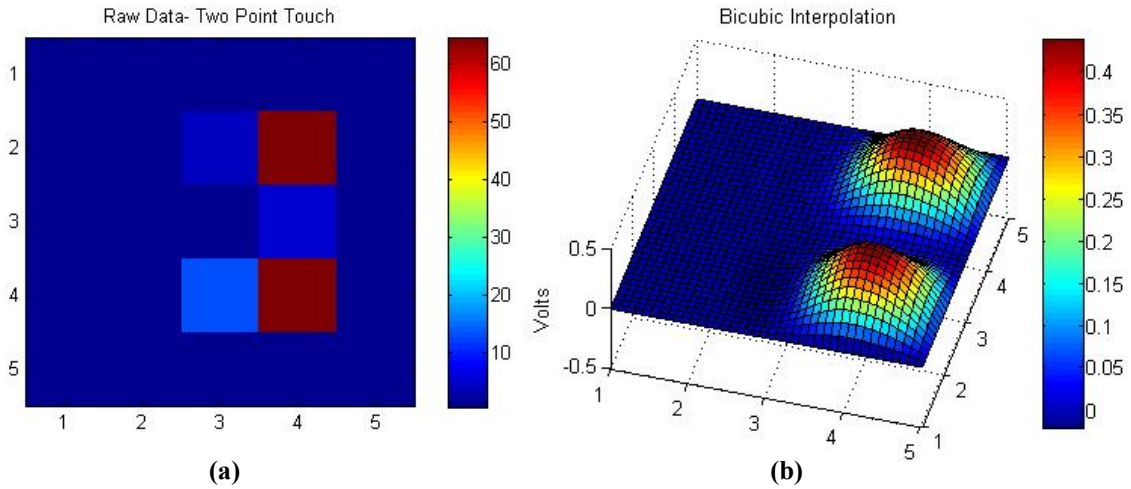

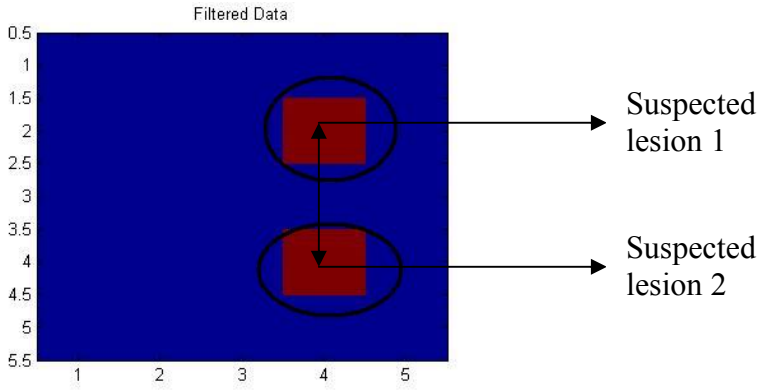

(c)

Figure 4.16 a) Raw data after stimulating two points for detecting distance between stimuli **b)** Bicubic interpolation of data after stimulating two points for distance detecting btw. stimuli **c)** Filtered data after stimulating two points for detecting distance between stimuli.

The "*distance.m*" file gives the distance between peak values and the output was: 2 pixels. This corresponds to 1 cm.

In a second test, the aesthesiometer was applied in an oblique angle.

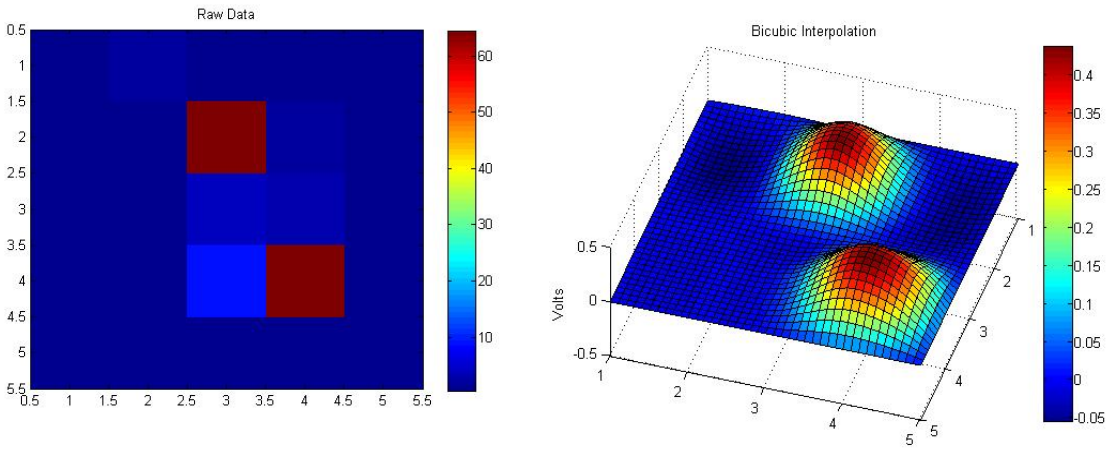

(a) **(b)**

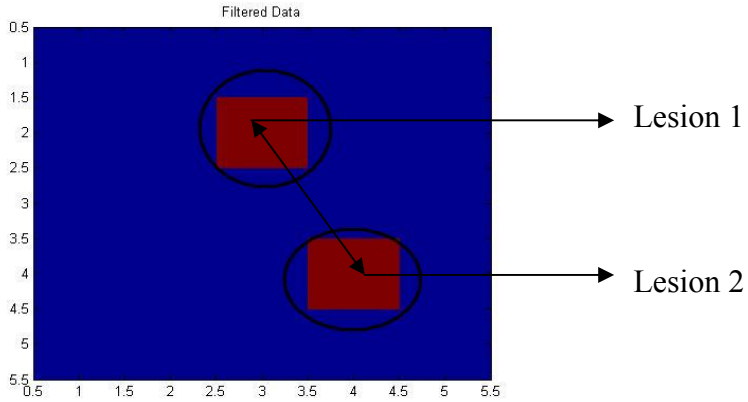

(c)

Figure 4.17 a) Raw data after stimulating two points for detecting distance between stimuli (1 cm) **c)** Filtered data after stimulating two points **b)** Bicubic interpolation of data after stimulating two points for distance detecting between stimuli (1 cm).

From the filtered data, the "*distance.m*" Matlab file can detect the distance between two lesions was 2.236 pixels. This corresponds to 1.118 cm (Fig. 4.15.c).

4.5.3 Discrimination of stimuli spaced 1.5 cm apart

In this case, the tester was adjusted to 1.5 cm and touched to the silicon surface (Fig. 4.17.a).

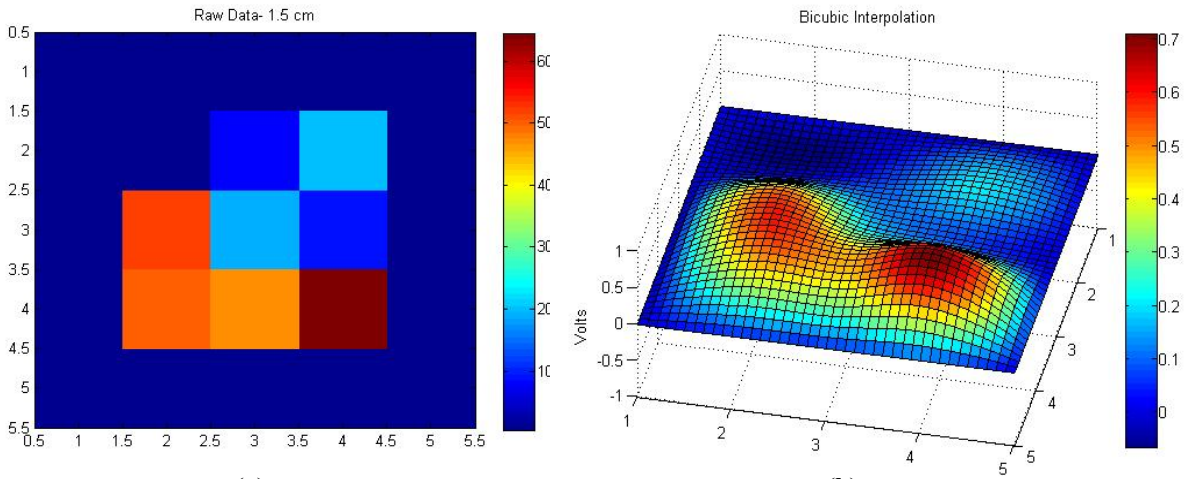

(a) **(b)**

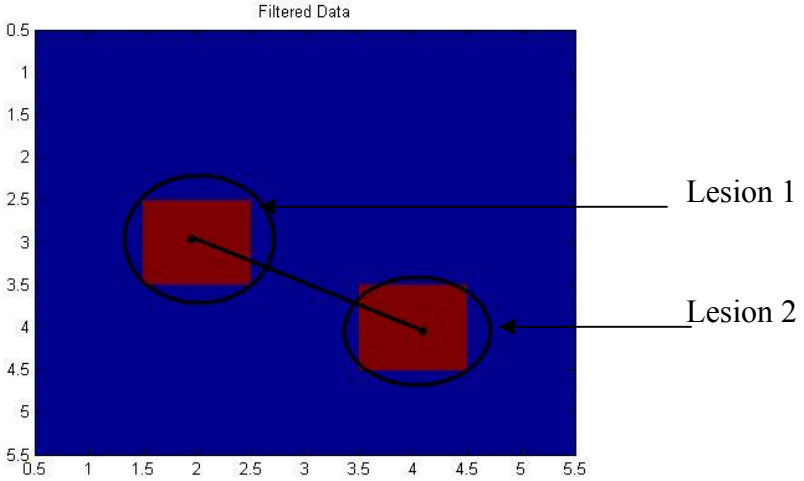

(c)

Figure 4.18 a) Raw data for detecting distance between stimuli (1.5 cm) **b)** Bicubic interpolation of data for detecting distance between stimuli (1.5 cm) **c)** Filtered data for detecting distance between stimuli (1.5 cm).

By distance.m, the distance was calculated as 2.36 pixels with corresponds to 1.118 cm.

Another experiment with aesthesiometer for 1.5 cm distance at an oblique angle (Fig. 4.18.a);

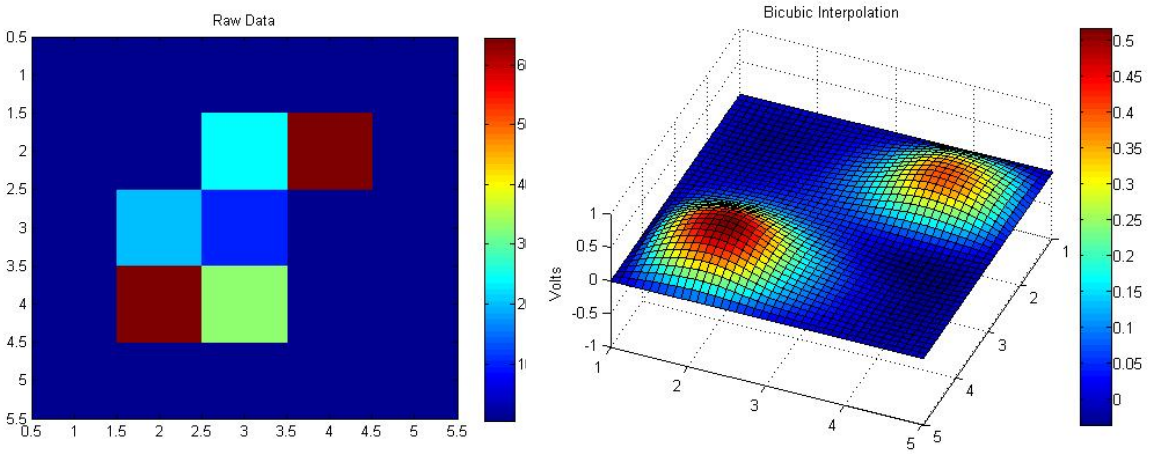

(a) **(b)**

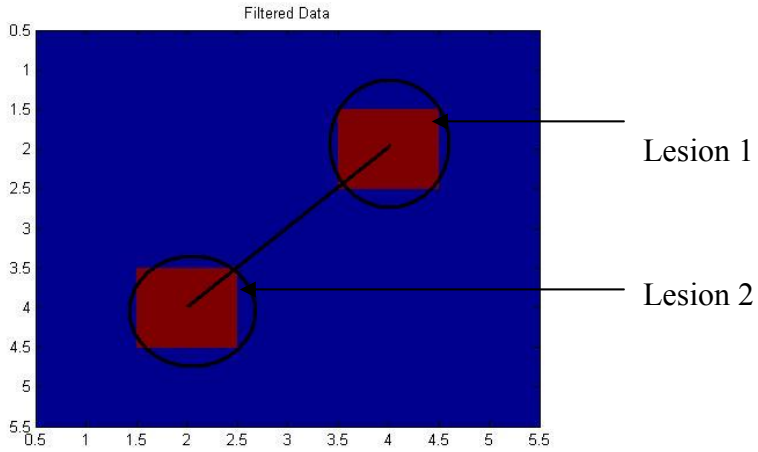

(c)

Figure 4.19 a) Raw data for detecting distance between stimuli (1.5 cm) no.2 **b)** Bicubic interpolation of data for detecting between stimuli (1.5 cm) no. 2 **c)** Filtered data for detecting distance between stimuli (1.5 cm) no.2.

By using "distance.m" we can find the distance between two suspected lesions as 2.83 pixels which corresponds to 1.4142 cm (Fig. 4.18.c).

4.6 Fingertip-contact experiment

In this experiment, tactile sensor was stimulated by an arbitrary object, i.e. fingertip. Figure 4.19.a shows the raw data and the contact point is defined as the peak point. In Figure 4.19.b bicubic interpolation of raw data was performed for more convenient data visualization.

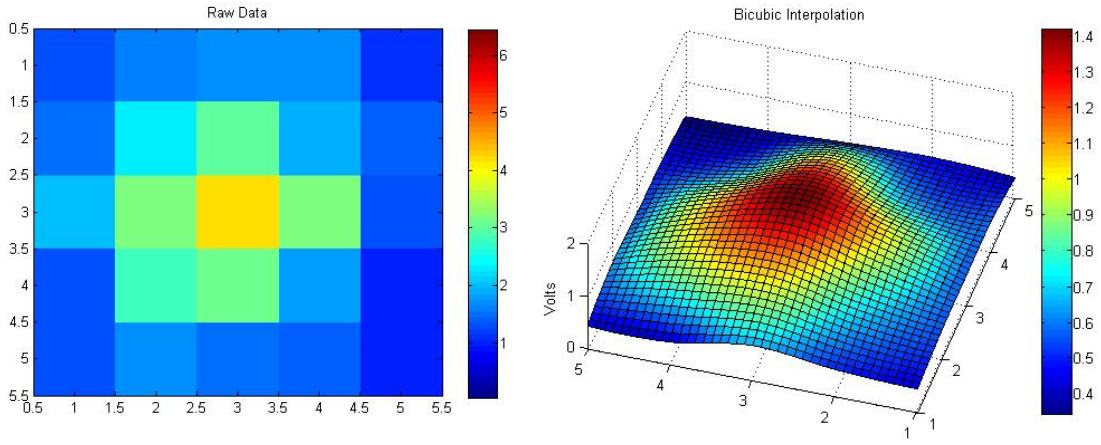

(a) **(b)**

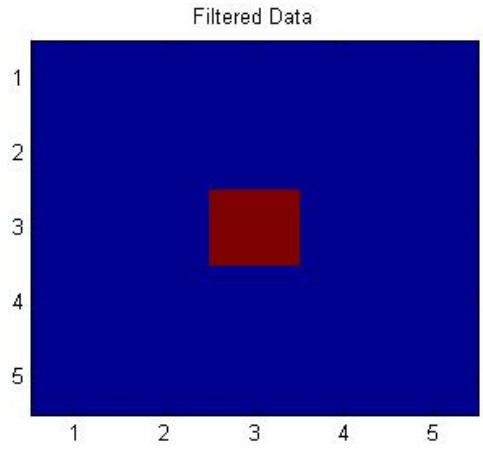

(c)

Figure 4.20 a) Raw Data of fingertip contact **b)** Bicubic Interpolation of fingertip contact **c)** Filtered Data-fingertip 3

The peak point corresponds to the “channel 13” in the tactile sensor array. According to the calibration curve, contact force was predicted as 767.4 gram-force (Fig. 4.19.c).

5. DISCUSSION

5.1 Resolution

According to the experimental results, the sensor has 5 mm spatial resolution. This is lower than the spatial resolution of the human fingertip (approximately 1 mm (10). This may not be convenient for some applications like finding small (1mm) tumors in arteries. But the lesions that are bigger than 5mm can be detected by the tactile sensor.

To increase the resolution of the optical tactile sensor, phototransistors should be located closer to each other and the size of the (active area) photosensitive elements must be much smaller (e.g. 0.1 mm for high resolution), and IR lights must be placed orderly between the photodiodes to supply balanced lightning on the backside of the tactile surface. The most effective solution is micromachining, because the design can be made very precise. High resolution may be helpful for laparoscopic applications and minimally invasive surgery. For automatic palpation, high resolution is essential, because according to tactile image of the lesion, the lump is determined to be malignant or not.

5.2 Cross-talk

Because of cross-talk, even if there is a single contact point, the neighboring sensors also produce relatively high outputs. Filtering can reduce the cross-talk and is useful to find the actual contact point. To reduce cross-talk of the sensor further a collimator design may be helpful. The IR lights can be sent via fiber-optic cables. The edge effect of the silicone rubber tactile surface can be eliminated by filling the gap between the sensors and surface by IR-light passing elements. This would limit the excessive deformation of the contact point relative to edges.

5.3 Linearity and Effects of Geometry

As seen in Table 4.1 the sensing elements are mostly linear. Of all 25 sensor elements, 6 elements were not linear (R^2<0.9). Specifically channels 3, 10, 11, 14, 15, 21

are not linear and this is not convenient for the ideal sensor requirements that is explained in the introduction section.

Of 6 non-linear elements, 5 were the elements located at the edges. Close to the edges of the sensor, channels are insensitive to the especially small forces because the silicone rubber surface cannot deform easily (Figure 5.1). The geometry is very important for sensitivity.

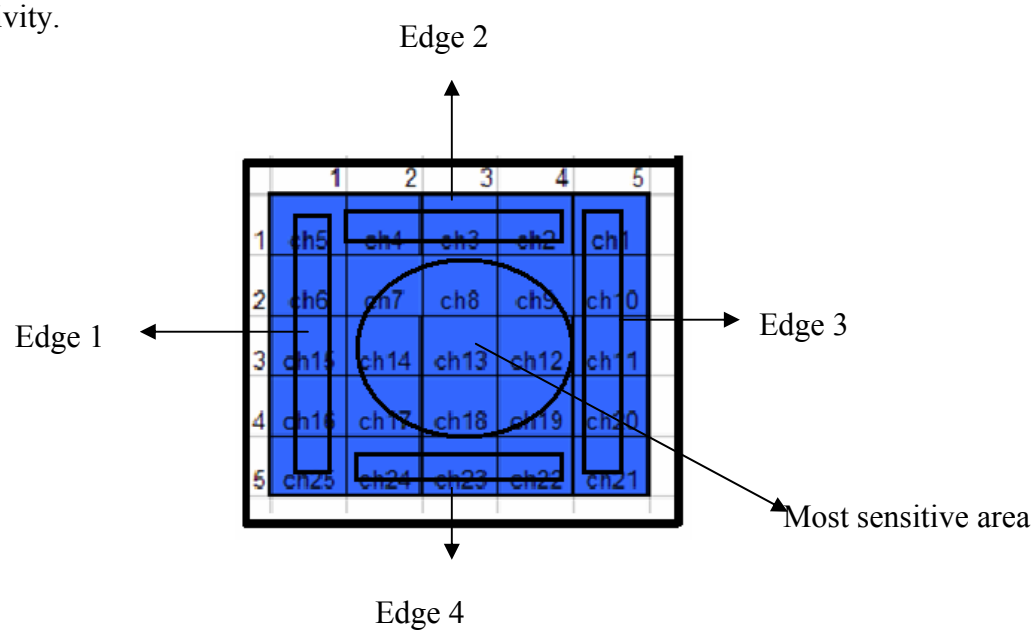

Figure 5.1 Effects of geometry on sensitivity.

The reason for nonlinearity of some edge sensor elements may also be that they receive less infrared light. Therefore, the placement of the sensors and infrared lights are very important as well. Additionally, the metal case of the sensor may reflect IR-light and produce noise. These unknown effects may be eliminated by using precise placement of the sensitive elements, using diffused light and using a light absorbing case for the system. A black bandage was covered in to the metal case to reduce the noise for the phototransistor.

Even though linearity is preferred, some non-linearities may be tolerated. For example, channel 14 which is not linear (R^2 = 0.7907) but calibrated by a high order polynomial.

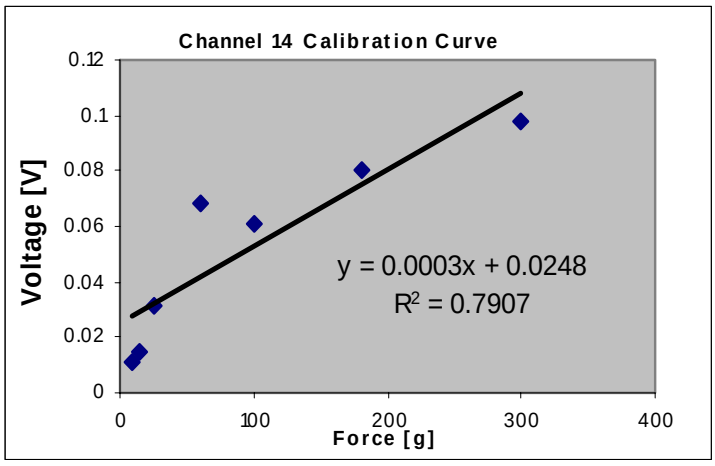

Figure 5.2 Linear Curve Fitting for Channel 14, $R^2 = 0.7907$.

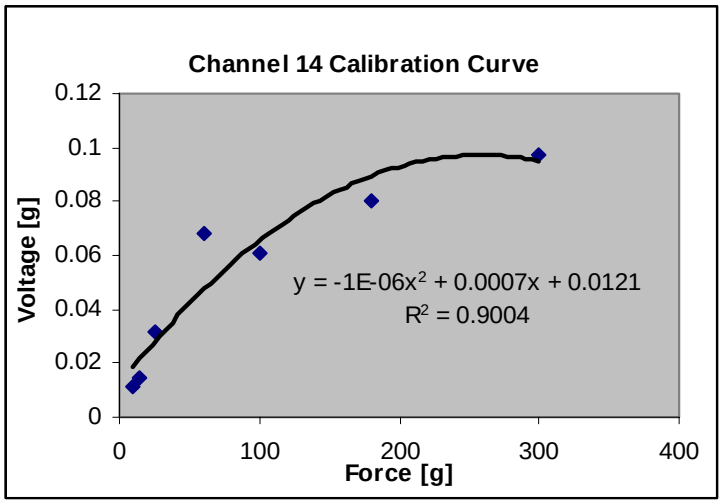

Figure 5.3 Second order polynomial for Channel 14, $R^2 = 0.9004$.

With the second order polynomial curve fitting quality factor became $R^2>0.9$.

5.4 Dynamic Range

The dynamic range of sensor was as 10 to 765 grams according to test results. Because of edge effects, small forces < 1 g-force cannot be distinguished, but at the center of the sensor, even 1g-force input can be detected. After elimination of edge effects, the dynamic range can be improved for major applications.

In the phantom experiment, it was shown that the sensor was able to distinguish different sizes of hard objects in the phantom 1 and 2. While lesion 1 in phantom 1 was detected in filtered data as 3 peak values, lesion 2 in phantom 2 was detected as 6 peak values. This may be used to compare the sizes of the lesions in the phantom. The actual sizes of the objects were 1 and 2 cm diameter.(Fig 4.7, Fig. 4.8).

By using the calibration equations, it was possible to predict forces. But in some trials, the predicted values were quite different from the actual forces. The silicone rubber tactile surface has the greatest effect on the precision.

5.5 Limitations of the Work

In this study, to test the optical array sensor, different types of experiments were conducted to see the performance of the test. Throughout the experiments, especially data acquisition part was more problematic. There were too much noise in some experiments, and sometimes the noises were bigger than the real data. Because of these problems, the calibration curves and experiment results were determined by one set of measurement, and repeatability, precision and accuracy of the sensor could not be tested properly. Additionally, because of time limit, the sensor could not be tested in clinic, but after solving the problems with the data acquisition card and geometrical problems of the sensor, the sensor is going to be tested in the clinic more than with phantom experiments.

6. CONCLUSION and FUTURE WORK

The aim of this study was to develop a prototype tactile sensor which can be used for tele-robotics applications and by clinicians to find lumps in soft tissues.

To evaluate the performance of the sensor, several experiments were conducted. Although the performance of the sensor was not sufficient for commercial applications, results were still in the range of tactile sensor requirements in terms of dynamic range and linearity. Especially spatial resolution can be increased by using smaller elements in the future.

The future work will involve designing a sensor with 10x10 and the update rate of the sensor will be increased by a more efficient communication protocol. Importantly, the geometry is going to be changed to eliminate edge effect.

APPENDIX

A.1 LISTING OF SOFTWARE

A.1.1 Realtime.m

```
% Real time data acquisition from Tactile Sensor
% DAQ 2 channels Analog Input
% Digital Outputs for Mux Control
% Adjustment of Analog Inputs

ai=analoginput('nidaq',1);
ch=addchannel(ai,0:1);

ai.SampleRate=100000;
ai.SamplesPerTrigger=10;
ai.TriggerType='Immediate';
ai.InputType = 'SingleEnded';

%digital  out channels adjustment
dio=digitalio('nidaq');
addline(dio, 0:7, 'out');

pval=[0 0 0 0 0 0 0 0 ];
putvalue(dio,pval);
%----calibration matrix-----
%ch1- ch17
pval=[ 0 0 0 0 1 1 0 0 ];
putvalue(dio,pval);
start(ai);
data=getdata(ai);
data=max(data);
ch1=data(1);
ch17=data(2);

%ch2- ch18
pval=[ 0 0 0 1 1 1 0 0 ];
putvalue(dio,pval);
start(ai);
data=getdata(ai);
data=max(data);
ch2=data(1);
ch18=data(2);
%ch3- ch19

pval=[ 0 0 1 0 1 1 0 0 ];
putvalue(dio,pval);
start(ai);
```

```
data=getdata(ai);
data=max(data);
ch3=data(1);
ch19=data(2);

%ch4- ch20
pval=[ 0 0 1 1 1 1 0 0 ];
putvalue(dio,pval);
start(ai);
data=getdata(ai);
data=max(data);
ch4=data(1);
ch20=data(2);

%ch5- ch21
pval=[ 0 1 0 0 1 1 0 0 ];
putvalue(dio,pval);
start(ai);
data=getdata(ai);
data=max(data);
ch5=data(1);
ch21=data(2);

%ch6- ch22
pval=[ 0 1 0 1 1 1 0 0 ];
putvalue(dio,pval);
start(ai);
data=getdata(ai);
data=max(data);
ch6=data(1);
ch22=data(2);

%ch7- ch23
pval=[ 0 1 1 0 1 1 0 0 ];
putvalue(dio,pval);
start(ai);
data=getdata(ai);
data=max(data);
ch7=data(1);
ch23=data(2);

%ch8- ch24
pval=[ 0 1 1 1 1 1 0 0 ];
putvalue(dio,pval);
start(ai);
data=getdata(ai);
data=max(data);
ch8=data(1);
ch24=data(2);
```

```
%ch9- ch25
pval=[ 1 0 0 0 1 1 0 0 ];
putvalue(dio,pval);
start(ai);
data=getdata(ai);
data=max(data);
ch9=data(1);
ch25=data(2);

%ch10
pval=[ 1 0 0 1 0 1 0 0 ];
putvalue(dio,pval);
start(ai);
data=getdata(ai);
data=max(data);
ch10=data(1);

%ch11
pval=[ 1 0 1 0 0 1 0 0 ];
putvalue(dio,pval);
start(ai);
data=getdata(ai);
data=max(data);
ch11=data(1);

%ch12
pval=[ 1 0 1 1 0 1 0 0 ];
putvalue(dio,pval);
start(ai);
data=getdata(ai);
data=max(data);
ch12=data(1);

%ch13
pval=[ 1 1 0 0 0 1 0 0 ];
putvalue(dio,pval);
start(ai);
data=getdata(ai);
data=max(data);
ch13=data(1);

%ch14
pval=[ 1 1 0 1 0 1 0 0 ];
putvalue(dio,pval);
start(ai);
data=getdata(ai);
data=max(data);
ch14=data(1);
```

```
%ch15
pval=[ 1 1 1 0 0 1 0 0 ];
putvalue(dio,pval);
start(ai);
data=getdata(ai);
data=max(data);
ch15=data(1);

%ch16
pval=[ 1 1 1 1 0 1 0 0 ];
putvalue(dio,pval);
start(ai);
data=getdata(ai);
data=max(data);
ch16=data(1);

clb= [ ch5 ch4 ch3 ch2 ch1;
       ch6 ch7 ch8 ch9 ch10;
       ch15 ch14 ch13 ch12 ch11;
       ch16 ch17 ch18 ch19 ch20;
       ch25 ch24 ch23 ch22 ch21];

   pause(0.001);

   % Main Program
      while 1==1

       %ch1- ch17
pval=[ 0 0 0 0 1 1 0 0 ];
putvalue(dio,pval);
start(ai);
data=getdata(ai);
data=max(data);
ch1=data(1);
ch17=data(2);

%ch2- ch18
pval=[ 0 0 0 1 1 1 0 0 ];
putvalue(dio,pval);
start(ai);
data=getdata(ai);
data=max(data);
ch2=data(1);
ch18=data(2);

%ch3- ch19
pval=[ 0 0 1 0 1 1 0 0 ];
putvalue(dio,pval);
start(ai);
```

```
data=getdata(ai);
data=max(data);
ch3=data(1);
ch19=data(2);

%ch4- ch20
pval=[ 0 0 1 1 1 1 0 0 ];
putvalue(dio,pval);
start(ai);
data=getdata(ai);
data=max(data);
ch4=data(1);
ch20=data(2);

%ch5- ch21
pval=[ 0 1 0 0 1 1 0 0 ];
putvalue(dio,pval);
start(ai);
data=getdata(ai);
data=max(data);
ch5=data(1);
ch21=data(2);

%ch6- ch22
pval=[ 0 1 0 1 1 1 0 0 ];
putvalue(dio,pval);
start(ai);
data=getdata(ai);
data=max(data);
ch6=data(1);
ch22=data(2);

%ch7- ch23
pval=[ 0 1 1 0 1 1 0 0 ];
putvalue(dio,pval);
start(ai);
data=getdata(ai);
data=max(data);
ch7=data(1);
ch23=data(2);

%ch8- ch24
pval=[ 0 1 1 1 1 1 0 0 ];
putvalue(dio,pval);
start(ai);
data=getdata(ai);
data=max(data);
ch8=data(1);
ch24=data(2);
```

```
%ch9- ch25
pval=[ 1 0 0 0 1 1 0 0 ];
putvalue(dio,pval);
start(ai);
data=getdata(ai);
data=max(data);
ch9=data(1);
ch25=data(2);

%ch10
pval=[ 1 0 0 1 1 0 0 0 ];
putvalue(dio,pval);
start(ai);
data=getdata(ai);
data=max(data);
ch10=data(1);

%ch11
pval=[ 1 0 1 0 1 0 0 0 ];
putvalue(dio,pval);
start(ai);
data=getdata(ai);
data=max(data);
ch11=data(1);

%ch12
pval=[ 1 0 1 1 1 0 0 0 ];
putvalue(dio,pval);
start(ai);
data=getdata(ai);
data=max(data);
ch12=data(1);

%ch13
pval=[ 1 1 0 0 1 0 0 0 ];
putvalue(dio,pval);
start(ai);
data=getdata(ai);
data=max(data);
ch13=data(1);

%ch14
pval=[ 1 1 0 1 1 0 0 0 ];
putvalue(dio,pval);
start(ai);
data=getdata(ai);
data=max(data);
ch14=data(1);
```

```
%ch15
pval=[ 1 1 1 0 1 0 0 0 ];
putvalue(dio,pval);
start(ai);
data=getdata(ai);
data=max(data);
ch15=data(1);

%ch16
pval=[ 1 1 1 1 1 0 0 0 ];
putvalue(dio,pval);
start(ai);
data=getdata(ai);
data=max(data);
ch16=data(1);


    map = [ ch5 ch4 ch3 ch2 ch1;
    ch6 ch7 ch8 ch9 ch10;
    ch15 ch14 ch13 ch12 ch11;
    ch16 ch17 ch18 ch19 ch20;
    ch25 ch24 ch23 ch22 ch21 ];


    pause(0.001);
    diff=(clb-map)

  for i=1:25
     if diff(i)<0
        diff(i)=0
      end
      end
          gain=30;
          image(gain*diff);
  end
```

A.1.2 Filter.m

```
%filtering
th=0.5; % global threshold
th2=0.85; % local threshold

mapx=mapfngr; % change the mapx name with the target

      figure;image(mapx*100)
      a= [1 1; 1 2;2 1;2 2]';
      [sa]=sub2ind([5 5],a(1:2:max(size(a))*2),a(2:2:max(size(a))*2))
      t=find(  (mapx(sa) >(max(max(mapx) )*th)) &( mapx(sa)>max(mapx(sa))*th2 ))
      if isempty(t),
      mapx(sa)=0;
      else
         t1=setdiff([1:max(size(a))],t)
      mapx(sa(t1))=0;
      end

      a=[1 2;1 1;2 1;2 2;2 3; 1 3]';
      [sa]=sub2ind([5 5],a(1:2:max(size(a))*2),a(2:2:max(size(a))*2))
       t=find(  (mapx(sa) >(max(max(mapx) )*th)) &( mapx(sa)>max(mapx(sa))*th2 ))
      t1=setdiff([1:max(size(a))],t)
      if isempty(t),
      mapx(sa)=0;
      else
         t1=setdiff([1:max(size(a))],t)
      mapx(sa(t1))=0;
      end

a=      [1 3;1 2;2 2;2 3;2 4;1 4]';
[sa]=sub2ind([5 5],a(1:2:max(size(a))*2),a(2:2:max(size(a))*2))
       t=find(  (mapx(sa) >(max(max(mapx) )*th)) &( mapx(sa)>max(mapx(sa))*th2 ))
      t1=setdiff([1:max(size(a))],t)
      if isempty(t),
      mapx(sa)=0;
      else
         t1=setdiff([1:max(size(a))],t)
      mapx(sa(t1))=0;
      end

a=[1 4; 1 3; 2 3;2 4;2 5;1 5 ]';
[sa]=sub2ind([5 5],a(1:2:max(size(a))*2),a(2:2:max(size(a))*2))
       t=find(  (mapx(sa) >(max(max(mapx) )*th)) &( mapx(sa)>max(mapx(sa))*th2 ))
      t1=setdiff([1:max(size(a))],t)
      if isempty(t),
      mapx(sa)=0;
      else
         t1=setdiff([1:max(size(a))],t)
```

```
      mapx(sa(t1))=0;
      end

a=       [1 5; 1 4; 2 4; 2 5]';
[sa]=sub2ind([5 5],a(1:2:max(size(a))*2),a(2:2:max(size(a))*2))
       t=find(  (mapx(sa) >(max(max(mapx) )*th)) &( mapx(sa)>max(mapx(sa))*th2 ))
      t1=setdiff([1:max(size(a))],t)
      if isempty(t),
      mapx(sa)=0;
      else
         t1=setdiff([1:max(size(a))],t)
      mapx(sa(t1))=0;
      end

a=       [2 1; 2 2; 1 1; 1 2; 3 2; 3 1]';
[sa]=sub2ind([5 5],a(1:2:max(size(a))*2),a(2:2:max(size(a))*2))
       t=find(  (mapx(sa) >(max(max(mapx) )*th)) &( mapx(sa)>max(mapx(sa))*th2 ))
      t1=setdiff([1:max(size(a))],t)
      if isempty(t),
      mapx(sa)=0;
      else
         t1=setdiff([1:max(size(a))],t)
      mapx(sa(t1))=0;
      end

a=       [2 2; 1 1; 2 1; 3 1 ;3 2; 3 3; 2 3; 1 3;1 2 ]';
[sa]=sub2ind([5 5],a(1:2:max(size(a))*2),a(2:2:max(size(a))*2))
       t=find(  (mapx(sa) >(max(max(mapx) )*th)) &( mapx(sa)>max(mapx(sa))*th2 ))
      t1=setdiff([1:max(size(a))],t)
      if isempty(t),
      mapx(sa)=0;
      else
         t1=setdiff([1:max(size(a))],t)
      mapx(sa(t1))=0;
      end

a=       [2 3; 1 3 ; 1 2; 2 2;3 2; 3 3; 3 4;2 4;1 4]';
[sa]=sub2ind([5 5],a(1:2:max(size(a))*2),a(2:2:max(size(a))*2))
       t=find(  (mapx(sa) >(max(max(mapx) )*th)) &( mapx(sa)>max(mapx(sa))*th2 ))
      t1=setdiff([1:max(size(a))],t)
     if isempty(t),
      mapx(sa)=0;
      else
         t1=setdiff([1:max(size(a))],t)
      mapx(sa(t1))=0;
      end

a=       [2 4;1 4;1 3;2 3;3 3; 3 4;3 5;2 5; 1 5]';
[sa]=sub2ind([5 5],a(1:2:max(size(a))*2),a(2:2:max(size(a))*2))
```

```
 t=find(  (mapx(sa) >(max(max(mapx) )*th)) &( mapx(sa)>max(mapx(sa))*th2 ))
t1=setdiff([1:max(size(a))],t)
if isempty(t),
mapx(sa)=0;
else
   t1=setdiff([1:max(size(a))],t)
mapx(sa(t1))=0;
end

a=       [2 5;3 5;1 5;1 4; 2 4; 3 4;]';
[sa]=sub2ind([5 5],a(1:2:max(size(a))*2),a(2:2:max(size(a))*2))
 t=find(  (mapx(sa) >(max(max(mapx) )*th)) &( mapx(sa)>max(mapx(sa))*th2 ))
t1=setdiff([1:max(size(a))],t)
if isempty(t),
mapx(sa)=0;
else
   t1=setdiff([1:max(size(a))],t)
mapx(sa(t1))=0;
end

a=       [3 1; 2 1; 2 2; 3 2;4 2;4 1]';
[sa]=sub2ind([5 5],a(1:2:max(size(a))*2),a(2:2:max(size(a))*2))
 t=find(  (mapx(sa) >(max(max(mapx) )*th)) &( mapx(sa)>max(mapx(sa))*th2 ))
t1=setdiff([1:max(size(a))],t)
if isempty(t),
mapx(sa)=0;
else
   t1=setdiff([1:max(size(a))],t)
mapx(sa(t1))=0;
end

a=  [3 2;2 2;2 1;3 1;4 1;4 2; 4 3; 3 3;2 3]';
[sa]=sub2ind([5 5],a(1:2:max(size(a))*2),a(2:2:max(size(a))*2))
 t=find(  (mapx(sa) >(max(max(mapx) )*th)) &( mapx(sa)>max(mapx(sa))*th2 ))
t1=setdiff([1:max(size(a))],t)
if isempty(t),
mapx(sa)=0;
else
   t1=setdiff([1:max(size(a))],t)
mapx(sa(t1))=0;
end

a=       [3 3;2 3;2 2;3 2; 4 2;4 3;4 4;3 4;2 4]';
[sa]=sub2ind([5 5],a(1:2:max(size(a))*2),a(2:2:max(size(a))*2))
 t=find(  (mapx(sa) >(max(max(mapx) )*th)) &( mapx(sa)>max(mapx(sa))*th2 ))
t1=setdiff([1:max(size(a))],t)
if isempty(t),
mapx(sa)=0;
else
```

```
        t1=setdiff([1:max(size(a))],t)
      mapx(sa(t1))=0;
      end


a=       [3 4;2 4;2 3;3 3;4 3;4 4;4 5;3 5;2 5]';
[sa]=sub2ind([5 5],a(1:2:max(size(a))*2),a(2:2:max(size(a))*2))
       t=find(  (mapx(sa) >(max(max(mapx) )*th)) &( mapx(sa)>max(mapx(sa))*th2 ))
      t1=setdiff([1:max(size(a))],t)
      if isempty(t),
      mapx(sa)=0;
      else
        t1=setdiff([1:max(size(a))],t)
      mapx(sa(t1))=0;
      end

a=       [3 5; 2 5;2 4;3 4;4 4;4 5 ]';
[sa]=sub2ind([5 5],a(1:2:max(size(a))*2),a(2:2:max(size(a))*2))
       t=find(  (mapx(sa) >(max(max(mapx) )*th)) &( mapx(sa)>max(mapx(sa))*th2 ))
      t1=setdiff([1:max(size(a))],t)
       if isempty(t),
      mapx(sa)=0;
      else
        t1=setdiff([1:max(size(a))],t)
      mapx(sa(t1))=0;
      end

   a=     [4 1;3 1;5 1;3 2; 4  2;5 2]';
   [sa]=sub2ind([5 5],a(1:2:max(size(a))*2),a(2:2:max(size(a))*2))
       t=find(  (mapx(sa) >(max(max(mapx) )*th)) &( mapx(sa)>max(mapx(sa))*th2 ))
      t1=setdiff([1:max(size(a))],t)
      if isempty(t),
      mapx(sa)=0;
      else
        t1=setdiff([1:max(size(a))],t)
      mapx(sa(t1))=0;
      end


a=       [4 2;3 2;5 2;3 1;4 1;5 1;3 3;4 3 ;5 3]';
[sa]=sub2ind([5 5],a(1:2:max(size(a))*2),a(2:2:max(size(a))*2))
       t=find(  (mapx(sa) >(max(max(mapx) )*th)) &( mapx(sa)>max(mapx(sa))*th2 ))
      t1=setdiff([1:max(size(a))],t)
     if isempty(t),
      mapx(sa)=0;
      else
        t1=setdiff([1:max(size(a))],t)
      mapx(sa(t1))=0;
      end
```

```
a=       [4 3;3 3;5 3;3 2;4 2;5 2;3 4;4 4;5 4]';
[sa]=sub2ind([5 5],a(1:2:max(size(a))*2),a(2:2:max(size(a))*2))
      t=find(  (mapx(sa) >(max(max(mapx) )*th)) &( mapx(sa)>max(mapx(sa))*th2 ))
     t1=setdiff([1:max(size(a))],t)
     if isempty(t),
     mapx(sa)=0;
     else
        t1=setdiff([1:max(size(a))],t)
     mapx(sa(t1))=0;
     end

a=       [4 4; 3 4;5 4;3 3;4 3; 5 3;3 5;4 5;5 5]';
[sa]=sub2ind([5 5],a(1:2:max(size(a))*2),a(2:2:max(size(a))*2))
      t=find(  (mapx(sa) >(max(max(mapx) )*th)) &( mapx(sa)>max(mapx(sa))*th2 ))
     t1=setdiff([1:max(size(a))],t)
     if isempty(t),
     mapx(sa)=0;
     else
        t1=setdiff([1:max(size(a))],t)
     mapx(sa(t1))=0;
     end

  a=     [4 5;3 5;5 5;3 4;4 4;5 4]';
  [sa]=sub2ind([5 5],a(1:2:max(size(a))*2),a(2:2:max(size(a))*2))
      t=find(  (mapx(sa) >(max(max(mapx) )*th)) &( mapx(sa)>max(mapx(sa))*th2 ))
     t1=setdiff([1:max(size(a))],t)
     if isempty(t),
     mapx(sa)=0;
     else
        t1=setdiff([1:max(size(a))],t)
     mapx(sa(t1))=0;
     end

a=       [5 1;4 1;4 2;5 2]';
[sa]=sub2ind([5 5],a(1:2:max(size(a))*2),a(2:2:max(size(a))*2))
      t=find(  (mapx(sa) >(max(max(mapx) )*th)) &( mapx(sa)>max(mapx(sa))*th2 ))
     t1=setdiff([1:max(size(a))],t)
     if isempty(t),
     mapx(sa)=0;
     else
        t1=setdiff([1:max(size(a))],t)
     mapx(sa(t1))=0;
     end

a=       [5 2;4 1;5 1;4 2;4 3;5 3]';
[sa]=sub2ind([5 5],a(1:2:max(size(a))*2),a(2:2:max(size(a))*2))
      t=find(  (mapx(sa) >(max(max(mapx) )*th)) &( mapx(sa)>max(mapx(sa))*th2 ))
     t1=setdiff([1:max(size(a))],t)
```

```
      if isempty(t),
      mapx(sa)=0;
      else
         t1=setdiff([1:max(size(a))],t)
      mapx(sa(t1))=0;
      end

a=       [5 3;4 2;5 2;4 4;5 4;4 3]';
[sa]=sub2ind([5 5],a(1:2:max(size(a))*2),a(2:2:max(size(a))*2))
       t=find(  (mapx(sa) >(max(max(mapx) )*th)) &( mapx(sa)>max(mapx(sa))*th2 ))
      t1=setdiff([1:max(size(a))],t)
      if isempty(t),
      mapx(sa)=0;
      else
         t1=setdiff([1:max(size(a))],t)
      mapx(sa(t1))=0;
      end

a=       [5 4;4 4 ;4 3 ;5 3;4 5;5 5]';
[sa]=sub2ind([5 5],a(1:2:max(size(a))*2),a(2:2:max(size(a))*2))
       t=find(  (mapx(sa) >(max(max(mapx) )*th)) &( mapx(sa)>max(mapx(sa))*th2 ))
      t1=setdiff([1:max(size(a))],t)
      if isempty(t),
      mapx(sa)=0;
      else
         t1=setdiff([1:max(size(a))],t)
      mapx(sa(t1))=0;
      end

a=       [5 5;4 5 ;4 4;5 4]';
[sa]=sub2ind([5 5],a(1:2:max(size(a))*2),a(2:2:max(size(a))*2))
       t=find(  (mapx(sa) >(max(max(mapx) )*th)) &( mapx(sa)>max(mapx(sa))*th2 ))
      t1=setdiff([1:max(size(a))],t)
      if isempty(t),
      mapx(sa)=0;
      else
         t1=setdiff([1:max(size(a))],t)
      mapx(sa(t1))=0;
      end
figure;image((mapx)*250);


% find the indices of region of interest
%run interpolation.m first
a=max(max(mapx));
[i]=find(mapx>= a*0.50);
i
IND = [i]
s = [5,5];
```

```
[I,J] = ind2sub(s,IND)

b=max(max(mapx));
[j]=find(mapx>= b*0.50);
j
IND = [j]
s = [5,5];
[I,J] = ind2sub(s,IND)

% end of the filter program..
```

A.1.3 Distance .m

```
% distance detection
%two_point.m, filter.m, distance.m
[i,j]=ind2sub([5 5],find(mapx>0))
for k=1:max(size(i))
for t=1:max(size(i))
   f(k,t)=norm([i(t) j(t)]-[i(k) j(k)])
end
end
```

A.1.4 Interpolation.m

```
% interpolation of experiment outputs
% raw data comes from realtim.m
% Outputs of Von Frey Hairs that have different grams
% data acquired by realtime.m and saved

mapfngr=[ 0.4518 0.5641 0.5812 0.5739 0.3883;
        0.5226 0.7692 1.0305 0.6593 0.4689;
        0.6764 1.0849 1.4139 1.0842 0.4347;
        0.4396 0.9646 1.0600 0.6227 0.3663;
        0.4444 0.5934 0.5128 0.4713 0.3419];

    [x,y] = meshgrid(1:1:5);
    z = mapfngr;
   [xi,yi] = meshgrid(1:0.1:5);
   zi3 = interp2(x,y,z,xi,yi,'bicubic');
   figure;    image(mapfngr*30);
  title('Raw Data');
  figure; surf(xi,yi,zi3);

% with 300 gr Von Frey Hair Touch
map300=[0.0195  0.0684  0.0977  0.1416   0.0586;
       0.0342  0.0855  0.0537  0.0366  0.1514;
       0.0781  0.2002  0.1392  0.2808   0.1758;
       0.0830  0.2466  0.3980  0.5421   0.0757;
```

```
       0.0488  0.0879  0.1709  0.1807   0];

[x,y] = meshgrid(1:1:5);
    z = map300;
[xi,yi] = meshgrid(1:0.1:5);
zi3 = interp2(x,y,z,xi,yi,'bicubic');
 figure;    image(map300*30);
title('Raw Data-300 gr Von Frey Hair');
 figure; surf(yi,xi,zi3);
title('Bicubic Interpolation- 300 gr Von Frey Hair');


% with 180 gr Von Frey Hair Touch
map180= [0.0366 0.0611 0.0952 0.0977 0.0562;
        0.0269 0.0733 0.0366 0.1734 0.1245;
        0.1563 0.3980 0.1368 0.0244 0.1416;
        0.2491 0.4689 0.3639 0.2369 0.0977;
        0 0.1685 0.1392 0.1123 0.0562];

[x,y] = meshgrid(1:1:5);
    z = map180;
[xi,yi] = meshgrid(1:0.1:5);
zi3 = interp2(x,y,z,xi,yi,'bicubic');

 figure;    image(map180*30);
 title('Raw Data-180 gr Von Frey Hair');
 figure; surf(yi,xi,zi3);
title('Bicubic Interpolation- 180 gr Von Frey Hair');


% with 100 gr Von Frey Hair Touch
map100=[0 0.0317 0.0366 0.0611 0;
       0 0.0513 0.0244 0.2295 0.0684;
       0.0024 0.0342 0.0879 0.0024  0.0830;
       0.0049 0.0537 0.0952 0.0977 0.0415
       0.0220 0.0366 0.0562 0.0586 0.0293];

[x,y] = meshgrid(1:1:5);
    z = map100;
[xi,yi] = meshgrid(1:0.1:5);
zi3 = interp2(x,y,z,xi,yi,'bicubic');

 figure;    image(map100*30);
 title('Raw Data-100 gr Von Frey Hair');
 figure; surf(yi,xi,zi3);
title('Bicubic Interpolation- 100 gr Von Frey Hair');
```

```
% with 15 gram Von Frey Hair Touch
map15=[0.0147 0.0220 0.0244 0.0342 0.00171;
       0.0244 0.0220 0.0147 0.0415 0.0293;
       0.0220 0.0293 0.0391 0.0098 0.0195;
       0.0147 0.0391 0.0513 0.0488 0.0122;
       0.0049 0.0122 0.0122 0.0122 0];

[x,y] = meshgrid(1:1:5);
    z = map15;
[xi,yi] = meshgrid(1:0.1:5);

zi3 = interp2(x,y,z,xi,yi,'bicubic');

 figure; image(map15*120);
 title('Raw Data-15 gr Von Frey Hair');
 figure; surf(yi,xi,zi3);
 title('Bicubic Interpolation- 15 gr Von Frey Hair');

 % Well Calibrated,Any Noise,  Touch By Hand
 maph2=[0 0 0 0 0 ;
        0 0 0 0 0 ;
        0 0 0.0611 0 0;
        0 0.2393 0.1783 0 0;
        0 0 0 0 0];
 [x,y] = meshgrid(1:1:5);
    z = maph2;
[xi,yi] = meshgrid(1:0.1:5);

zi3 = interp2(x,y,z,xi,yi,'bicubic');
 figure; image(maph2*30);
 title('Raw Data- finger tip');
 figure; surf(yi,xi,zi3);
 title('Bicubic Interpolation- finger tip');

 % compare the peaks of the Responses to the  Von Frey Hairs
a=max(max(map300));
b=max(max(map180));
c=max(max(map100));
d=max(max(map15));
peaks = [d c b a];
grams=[15 100 180 300];
figure; plot(grams,peaks,'-o');

set(gca,'XTick',[15 100 180 300])
xlabel('Grams');
ylabel('Volts');
title('Calibration Plot for ch1');

p = polyfit(grams,peaks,1)
```

```
x2 = 0:.1:310;
y2 = polyval(p,x2);
plot(grams,peaks,'-o',x2,y2)
grid on
```

A.1.5 Two_point.m

```
% two point m file
% two point discrimination

tp1=[0 0 0 0 0 ;
    0 0 0.0147 0.4347 0;
    0 0 0 0.0195 0;
    0 0 0.0464 0.4371 0;
    0 0 0 0 0];
[x,y] = meshgrid(1:1:5);
    z = tp1;
[xi,yi] = meshgrid(1:0.1:5);
zi3 = interp2(x,y,z,xi,yi,'bicubic');
 figure; image(tp1*300);
 title('Raw Data');
 figure; surf(xi,yi,zi3);
  title('Bicubic Interpolation');
   a=max(max(tp1));
[i]=find(tp1>= a*0.70)
IND = [i]
s = [5,5];
[I,J] = ind2sub(s,IND)

% Two point for 0.5cm
tp05=[0 0 0 0 0 ;
     0 0 0 0 0 ;
     0 0.5226 0.0659 0 0 ;
     0 0.4347 0.2906 0 0 ;
     0 0.1172 0 0 0];

[x,y] = meshgrid(1:1:5);
    z = tp05;
[xi,yi] = meshgrid(1:0.1:5);
zi3 = interp2(x,y,z,xi,yi,'bicubic');
 figure; image(tp05*200);
 title('Raw Data');
 figure; surf(xi,yi,zi3);
  title('Bicubic Interpolation');
%%%%%
  tp3=[0 0.0147 0 0 0 ;
    0 0 0.4347 0.0124 0;
    0 0 0.0222 0.0195 0;
```

```
    0 0 0.0464 0.4371 0;
    0 0 0 0 0];
  [x,y] = meshgrid(1:1:5);
    z = tp3;
[xi,yi] = meshgrid(1:0.1:5);
zi3 = interp2(x,y,z,xi,yi,'bicubic');
 figure; image(tp3*200);
 title('Raw Data');
 figure; surf(yi,xi,zi3);
  title('Bicubic Interpolation');
  %%%%%%%%%%%%%%
  tp15=[0 0 0 0 0;
       0 0 0.0855 0.2027 0;
       0 0.5250 0.1905 0.0952 0;
       0 0.5031 0.4713  0.6911 0;
       0 0 0 0 0];
    [x,y] = meshgrid(1:1:5);
     z = tp15;
[xi,yi] = meshgrid(1:0.1:5);
zi3 = interp2(x,y,z,xi,yi,'bicubic');
 figure; image(tp15*200);
 title('Raw Data');
 figure; surf(yi,xi,zi3);
  title('Bicubic Interpolation');
  %%%%%%%%%%%%%%
  tps1=[0 0 0 0 0;
       0 0  0.1209 .4029 0;
       0 0.1025 0.0537 0 0;
       0 0.51530 0.1685 0 0;
       0 0 0 0 0];

     [x,y] = meshgrid(1:1:5);
     z = tps1;
[xi,yi] = meshgrid(1:0.1:5);
zi3 = interp2(x,y,z,xi,yi,'bicubic');
 figure; image(tps1*200);
 title('Raw Data');
 figure; surf(yi,xi,zi3);
  title('Bicubic Interpolation');
```

REFERENCES

1. Lang, P., "Optical Tactile Sensor for Medical Palpation," *The Thirty-Fourth London District Science and Technology Conference*, pp. 1-5, Mar 2004.

2. Kitagawa, M., A. M. Okamura, B. T. Bertha, V. L. Gott, and W. A. Baumgartner, "Analysis of Suture Manipulation Forces for Teleoperation with Force Feedback," *Proc. of the Fifth Int. Conf. on Medical Image Computing*, Vol. 2488, pp. 155-162, 2002.

3. Ohtsuka, T., A. Furuse, T. Kohno, J. Nakajima, K. Yagyu, and S. Omata, "New Tactile Sensor Techniques for Localization of Pulmonary Nodules. International Surgery," *The Int. J. of Robotics Research*, Vol. 19(7), pp. 636-643, June 1997.

4. Menciassi, A., A. Eisinberg, C. Anticoli, M. C. Carrozza, and P. Dario, "Force Feedback-based microinstrument for measuring tissue properties and pulse in microsurgery", *Proc. of the IEEE Int. Conf. on Robotics and Automation*, pp. 626-631, May 2001.

5. Wang, Y., C. Nguyen., R. Srikanchana, Z. Geng, and M. T. Freedman, "Tactile Mapping of Palpable Abnormalities for Breast Cancer Diagnosis," *Proc. of the Int. Conf. on Robotics and Automation*, pp. 1305-1309, May 1999.

6. Zeng, J., Y. Wang, M. T. Freedman, and S. K. Mun, "Finger Tracking for Breast Palpation Quantification using Color Image Features," *SPIE J. of Opt. Eng*., Vol. 36(12), pp. 3455-3461, Dec. 1997.

7. Haagensen, C. D., *Diseases of the Breast*, Philadelphia: Saunders, 3rd ed., 1986.

8. Howe, R. D., W. J. Peine, D. A. Kontarinis, and J. Son, "Remote Palpation Technology," *IEEE Eng. in Medicine and Biology*, Vol. 14(3), pp. 318-323, May/June 1995.

9. Dario, P., and M. Bergamasco, "An Advanced Robot ,System for Automated Diagnosis Tasks through Palpation," *IEEE Trans. Biomed. Eng*., Vol. 35(2), pp. 118-126, Feb. 1988.

10. Webster, J. G., ed., *Tactile Sensor for Robotics and Medicine*, New York: John Wiley & Sons, pp. 1-15, 1988.

11. Fearing, R. S., "Tactile Sensing Mechanisms," *Intl. J. Robotics Research*, Vol. 9(3), pp. 3-23, 1990.

12. Wellman, P. S., "A Biomechanical Model for tactile Mapping of Palpable Abnormalities," *Harvard Robotics Lab Technical Report 96-002*, 1996.

13. Dargahi, J., and S. Najarian, "An integrated force-position tactile sensor for improving diagnostic and therapeutic endoscopic surgery," *Bio-Medical Materials and Engineering*, Vol. 14, pp. 151- 166, 2004.

14. Hannaford, B., J. Trujillo, M. Sinanan, M. Moreyra, J. Rosen, J. Brown, R. Leuschke, and M. MacFarlane, "Computerized endoscopic surgical grasper," *Medicine Meets Virtual Reality*, Vol. 50, pp. 265–271, 1998.

15. Rininsland, H. H., "Basics of robotics and manipulators in endoscopic surgery," *Endoscopic Surgery and Allied* Technologies, Vol. 1, pp. 154–159, 1993.

16. Melzer, H.H., M. O. Schurr, W. Kunert, G. Buess, U. Voges, and J. U. Meyer, "Intelligent surgical instrument system," *Endoscopic Surgery and Allied Technologies*, Vol. 1, pp. 165–170, 1993.

17. Bhoyrul, S., and T. Mori, eds., *Fundamentals of Laparascopic Surgery*, New York: Churchill-Livingston, 1995.

18. Dargahi, J., M. Parameswaran, and S. Payandeh, "A micromachined piezoelectric tactile sensor for and endoscopic grasper – theory, fabrication, and experiments," *Journal of Microelectromechanical Systems*, Vol. 9(3), pp. 329–335, 2000.

19. Brouwer, I., J. Ustin, L. Bentley, A. Sherman, N. Dhruv, and F. Tendick, "Measuring in vivo animal soft tissue properties for haptic modeling in surgical simulation," *Medicine Meets Virtual Reality*, Vol. 81, pp. 69–74, 2001.

20. Wagner, C. R., N. Stylopoulos, and R. D. Howe, "The role of force feedback in surgery: analysis of blunt dissection," *The 10th Symposium on Haptic Interfaces for Virtual Environment and Teleoperator Systems*, pp. 73–79, 2002.

21. Fearing, R.S., G. Moy, and E. Tan, "Some basic issues in tele-taction," *IEEE Int. Conf. on Robotics and Automation*, pp. 3093–3099, 1997.

22. Eklund, A., A. Bergh, and O. A. Lindahl, "A catheter tactile sensor for measuring hardness of soft tissue: measurement in a silicone model and in an in vitro human prostate model," *Medical & Biological Engineering & Computing*, Vol. 37, pp. 618–624, 1999.

23. Howe, R.D., W. J. Peine, D. A. Kontarinis, and J. S. Son, "Remote palpation technology," *Proc. of the IEEE Eng. in Medicine and Biology Magazine*, Vol. 14(3), pp. 318–323, 1994.

24. Dargahi, J., "An endoscopic and robotic tooth-like compliance and roughness tactile sensor," *Journal of Mechanical Design*, Vol. 124, pp. 576–582, 2002.

25. Miyagii, K., A. Furuse, J. Nakajima, T. Kohno, T. Ohtsuka, K. Yagyu, T. Oka, and S. Omata, "The stiffness of lymph nodes containing lung carcinoma metastases: a new diagnostic parameter measured by a tactile sensor," *Cancer*, Vol. 80, pp. 1920–1925, 1997.

26. Dargahi, J., "A study of the human hand as an ideal tactile sensor used in robotic and endoscopic applications," *Proc. of the CSME International Conference,* pp. 21–22, 2001.

27. Crago, E., J. Nakai, and H. J. Chizeck, "Feedback regulation of hand grasp opening and contact force during stimulation of paralyzed muscle," *IEEE Trans. on Biomed. Eng.*, Vol. 38, pp. 17–28, 1991.

28. Dargahi, J., A. Eastwood, and I. J. Kemp, "Combined force and position polyvinylidene fluoride (PVDF) robotic tactile sensing system," *Proc. of SPIE Int. Conf.,* pp. 20–25, 1997.

29. AANA (Arthroscopy Association of North America), “Scope Mechanics and Comprehensive Diagnostic Arthroscopy,” 2003. Available : www.aana.org.

30. Dargahi, J., S. Payandeh, and M. Parameswaran, “A micromachined piezoelectric teeth-like laparoscopic tactile sensor: theory, fabrication, and experiments,” *Proc. of the IEEE Int. Conf. on Robotics and Automation*, pp. 299–340, 1999.

31. Ohka, M., Y. Mitsuya, I. Higashioka, and H. Kabeshita, “An Experimental Optical Three-axis Tactile Sensor for Micro-Robots,” *Robotica*, Vol. 23, pp. 457-465, 2005.

32. Nicholls, H. R., *Advanced Tactile Sensing for Robotics*, Singapore: World Scientific, 1992.

33. Mott, D. H., M. H. Lee, and H. R. Nicholls, “An Experimental Very High Resolution Tactile Sensor Array,” *Proc. of the 4th Int. Conf. On Robot Vision and Sensory Control*, pp. 241–250, 1984.

34. Tanie, K., K. Komoriya, M. Kaneko, S. Tachi, and A. Fujiwara, “A High Resolution Tactile Sensor Array,” *Robot Sensors*, Vol. 2: Tactile and Non-Vision, UK, pp. 189–198, 1986.

35. Nicholls, H. R., “Tactile Sensing Using an Optical Transduction Method,” *Traditional and Non-traditional Robot Sensors*, pp. 83–99, 1990.

36. Maekawa, H., K. Tanie, K. Komoriya, M. Kaneko, C. Horiguchi, and T. Sugawara, “Development of Finger-shaped Tactile Sensor and Its Evaluation by Active Touch,” *Proc. of the IEEE Int. Conf. on Robotics and Automation*, pp. 1327– 1334, 1992.

37. Kamiyama, K., H. Kajimoto, N. Kawakami, and S. Tachi, “Evaluation of a Vision-based Tactile Sensor,” *Proc. of the IEEE Int. Conf. on Robotics and Automation*, Vol. 2, pp. 1542-1547, April 2004.

38. Tima, J., “Tactile Sensor Array Signal and Data Processing,” *Workshop on metrological aspects of the quality assurance-accreditation and certification in new millenium, Bratislava*, pp. 137-145, Mar 2001.